Biomechanical loading behaviour of a knee joint distraction device as treatment for osteoarthritis

A FINITE ELEMENT ANALYSIS STUDY

Van Duijnhoven H.J.H.

Student nr: 5407907

Specialization: Finite element modelling of biological tissues

Department: Biomechanical engineering

Faculty: Mechanical, Maritime and Material engineering (3ME)

University: Technical University Delft







Table of Contents

1 INTRODUCTION	3
1.1 Phone was government	_
1.1 PROBLEM STATEMENT	
1.2 OBJECTIVES	
2 BACKGROUND	8
2.1 SURGICAL PROCEDURE	8
2.1.1 PIN POSITION	8
2.1.2 PIN LENGTH	
2.2 THEORETICAL CALCULATIONS	10
2.2.1 THEORETICAL PIN DEFLECTION	
2.2.2 THEORETICAL JSW DECREASE	
2.2.3 THEORETICAL PARAMETER ADJUSTMENTS	
2.3 LOADING IN KJD TREATMENT	15
3 METHODS & MATERIALS	16
3.1 CREATION OF THE ORIGINAL MODEL	16
3.1.1 DATA DESCRIPTION	16
3.1.2 MODEL CREATION WORKFLOW	16
3.1.3 DISTRACTION	18
3.1.4 MESH CONVERGENCE	19
3.1.5 MATERIAL ASSIGNMENT	
3.1.6 PIN-BONE CONNECTION	
3.1.7 MONOTUBE SPRING MODELING	
3.1.8 BOUNDARY CONDITIONS	
3.1.9 LOADING CONDITIONS	
3.1.10 JSW AND ROTATION CALCULATION	
3.1.11 JOINT SPACE WIDTH DETERMINATION	
3.2 FRAME ADJUSTMENTS	
3.2.1 ADJUSTED PIN THICKNESS	
3.2.2 ADJUSTED EFFECTIVE PIN LENGTH	
3.2.3 CONVERGING PINS	
3.2.4 ROTATED PINS	
3.3 INDIVIDUAL PIN DIFFERENCES	
3.3.1 STRESS CONCENTRATIONS	
3.3.2 MICROMOTIONS	
5.4 RELATIONS FRAME PARAMETERS	33
4 RESULTS	34
4.4.37	•
4.1 VALIDATION	
4.2 JSW MEASUREMENTS	







4.4 FORCE VS DISPLACEMENT PLOTS JSW	37
4.4.1 PIN THICKNESS VARIATIONS	
4.4.2 PIN LENGTH VARIATIONS	38
4.4.3 INSERTION ANGLE: CONVERGING PINS	39
4.4.4 INSERTION ANGLE: ROTATED PINS	40
4.5 KNEE ROTATIONS	41
4.6 STRESS CONCENTRATIONS	42
4.7 MICROMOTIONS	44
4.8 RELATIONS FRAME PARAMETERS	45
5 DISCUSSION	48
5.1 LIMITATIONS	10
5.2 INTERPRETATION	
5.3 CONCLUSIONS	
5.4 COMPARISON OTHER PAPERS	
5.5 FURTHER RESEARCH	52
6 BIBLIOGRAPHY	53
7 APPENDIX	55
7.1 MODEL CREATION STEPS	55
7.2 ADDITIONAL FIGURES	







1 INTRODUCTION

Osteoarthritis (OA) is a degenerative joint disease characterized by pain, swelling, joint stiffness and deformation of the bones around the joint. Knee OA is the fourth leading cause of disability worldwide, affecting about 6% of the total adult population with an incidence of 100-240 thousand people yearly (Mahir et al., 2016, D'Ambrosia, 2005). OA hampers the ability to perform daily tasks like walking and climbing stairs with a large impact on a patient's quality of life (Mahir et al., 2016). Knee OA is caused by repetitive wear and tear of the knee joint cartilage. This leads to the deterioration of cartilage quality and thickness (Knecht et al., 2006).

After careful conservative treatment strategies, a total knee arthroplasty (TKA) is a common treatment option. In end-stage OA patients aged above 65 years, it improves the patient's quality of life and diminishes knee symptoms. TKA is a fast and streamlined treatment with a surgery time between 1 and 2 hours and a recovery time of several weeks. A disadvantage of TKA, however, is the risk of revision surgery, especially when the primary prosthesis was placed in patients aged below 65 years. Revision surgery following arthroplasty is typically associated with more complications and a less favourable cost-effectiveness when compared to the initial procedure (Weber et al., 2018). Additionally, the longevity of a knee implant is often influenced by the level of activity of the patient (Bayliss et al., 2017). This creates a challenge for younger and more active individuals who have end-stage knee OA and no conservative option left. Therefore, alternatives to TKA must be examined.

Knee joint distraction (KJD) is an alternative treatment that aims to preserve the knee joint and extend its lifetime. This treatment is generally performed in young patients below the age of 60. KJD is typically performed with a bilaterally applied external fixation frame which is fixed in the femur and tibia using bone pins. The external fixator enlarges the joint space width (JSW) between the femoral and tibial bone by exerting force. The JSW is the distance between the femur bone and the tibia bone. In the case of OA, the JSW can be dramatically small because of the deterioration of joint tissue like cartilage and meniscus. Often, there is bone-on-bone contact, which leads to more pain and inflammation in the joint. Using KJD treatment, the remaining joint cartilage is unloaded, further damage is prevented, and cartilage repair is stimulated (Jansen, Mastbergen, et al., 2020). The external fixator is 6 weeks in situ while the patient is allowed to walk with crutches. In an open uncontrolled prospective study performed by van der Woude et al. (2017), KJD resulted in a prolonged clinical benefit for up to at least 5 years and delayed the need for TKA. WOMAC (Western Ontario and McMaster Universities Arthritis Index) and VAS (Visual Analogue Scale score) pain scores were lower compared to baseline and there was still an increased joint space width in the most affected compartment. In a study performed by Jansen et al. (2021), where KJD was compared to TKA and osteotomy, KJD realized a sustained clinical improvement as well as an increase in cartilage thickness. Therefore, they suggested that the clinical outcomes for KJD are similar to those of TKA and osteotomy.

ArthroSave (Culemborg, Netherlands) is a company that produces KJD frames. The ArthroSave 'KneeReviver' (Figure 1) is a modified bilateral external frame that is based on a basic monotube system that was used before in clinical settings (Intema et al., 2010). Each side is attached to the femur by two parallel pins and the tibia by two parallel pins. This makes a total of 8 pins that penetrate the skin and soft tissues and secure the frame within the bones. Both sides of the frame consist of:







- A. Two blocks to clamp the pins. These parts have holes for the pins and screws to tighten the pins in the blocks.
- B. Two ball and socket joints. These joints are flexible during the placement of the frame. After the surgery, the joints are fixated with a screw.
- C. One rigid connecting part. The rigid part is the connector between the upper and lower pins. Its orientation depends on the patients' morphology.
- D. One monotube containing a spring of stiffness 144 N/mm.

While wearing the ArthroSave frame, patients are instructed to walk and stand on the treated leg with crutches, meaning exerting force on the KJD fixator. This leads to intermittent joint fluid pressures which is proven to be beneficial for cartilage repair (van Valburg et al., 1998). To ensure this intermittent fluid pressure, the ArthroSave frame has built-in springs that allow for some force-dependent movement within the JSW. The springs are designed to lock at 3.2 mm deformation to avoid loading in the articular surface structures.

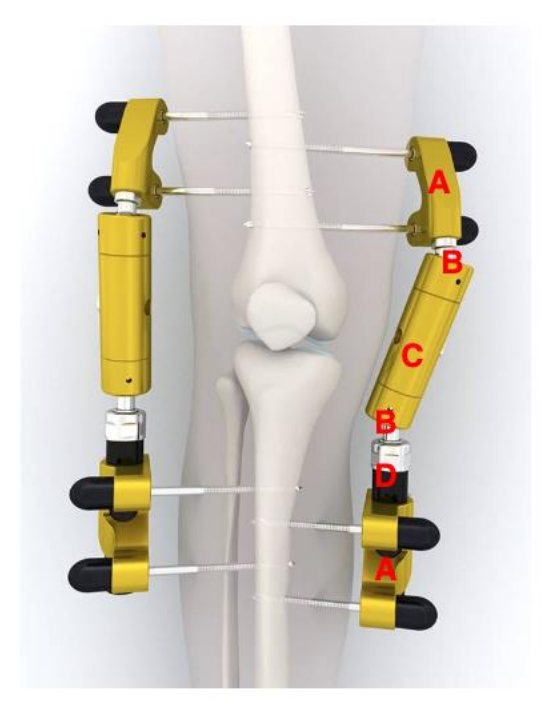


Figure 1 Schematic overview of the knee joint with ArthroSave Kneereviver distraction frame attached. Letters (A,B,C,D,E) represent different parts of the frame. (ArthroSave,unknown)







1.1 PROBLEM STATEMENT

ArthroSave is aiming to expand its services internationally. In some countries however, residents have different demographic characteristics when it comes to physical health. Take for instance the United States of America compared to Europe. Monitoring research revealed that 30.4 % of adult Americans (>20 years) are obese (BMI>30) (Baskin et al., 2005). While in Europe, 22 % of adults are obese. For both regions, these numbers are still increasing (WHO, 2022). These findings lead to three important factors with respect to knee OA and KJD:

- 1. Obesity leads to a bigger incidence of knee OA in young patients (Lee and Kean, 2012).
- 2. Higher expected patient bodyweight leads to a higher applied force to the frame during walking or standing.
- 3. Patients with more subcutaneous fat tissues are expected to get longer pin lengths in KJD treatment.

Points two and three are both expected to lead to more pin deformation and a bigger chance of bone-on-bone contact within the knee joint during KJD with a less efficient KJD treatment as result. Pin bending might influence the relative distance between femur and tibia such that the distracted JSW could be negated. On the other hand, pin thickness (Figure 2) should be minimized to reduce the chance on pin tract infections. Patient specific pins could provide a solution to this problem.

Simple estimations of pin bending could be performed analytically. However, because of the pin length, number of pins and complex geometry of the ArthroSave frame and femoral and tibial bones, a computational model is more accurate. Finite Element Models (FEM) are an accurate in silico model and can provide valuable biomechanical information of biological structures like the knee joint (Hölzer et al., 2013, Haut Donahue, 2002). Therefore, this project aims to develop a FEM of the knee joint treated with KJD.

FEM analysis also allows to modify several frame parameters. Studies report various pin diameters used in clinical research (Seitz et al., 1990, Terzini et al., 2019). Besides, as mentioned, pin lengths are dependent on characteristics of each patient. Therefore, pin diameter and pin length are modified in this research (Figure 2 and 3).

Moreover, insertion angles of the bone pins are mostly determined by anatomical structures. Nonetheless, modifications can be performed. Lenarz et al. (2008) believed that small modifications of pin angles could be executed without detrimental consequences. Once the pins are surgically placed in a converging angle (Figure 5), the deformation could be less due to a decreased moment arm. This might influence the total stiffness of the frame. Furthermore, changing the alignment of the femoral and tibial pins (Figure 4) could also alter the frame stiffness. It is expected that the stiffness is increasing when the angular difference between the femoral and tibial pins decreases. In this research, these parameters are varied to gain more insight in the mechanical response of the frame.

While loading the affected knee in KJD, there could be relative movements between the femur and tibia. Relative rotations might occur in exo- and/or endo, ad- or abduction, and flexion or extension directions. Excessive rotation should be limited by the surrounding ligaments, muscles, and tendons. This could have impact on the effectiveness of the KJD treatment. Because these relative rotations are unknown during KJD treatment, they are also examined.







Additionally, during KJD treatment, the most abundant complications are pin tract infections (Jansen, van Egmond, et al., 2020). As explained in Wolf's law, mechanotransductor cells within bone tissue can detect mechanical stimuli and convert them into electrochemical signals. These electrochemical signals could induce bone tissue remodelling but also inflammatory bone tissue reactions (Frost, 1994). Therefore, stress concentrations could lead to inflammation or loosening of pins. Also, there is a possibility of micromotions between the bones and pins, which could affect pin tract infections. Investigating the stress concentrations and micromotions in the bone pin interactions possibly provides valuable insights to overcome inflammation and pin loosening (Aro et al., 1993).

This research thus aims to investigate the mechanical behaviour of the KJD frame in situ with different parameter alterations. These alterations are pin diameter (Figure 2), pin length (Figure 3), and pin angles (Figures 4 and 5). Of interest are changes in JSW, joint rotations and local stresses in the bone-pin interactions during loading. The current KJD treatment has predefined pin diameters, pin lengths, and pin angles. However, knowledge on the mechanical behaviour of the KJD frame could be used in the process of implementing patient specific pins.

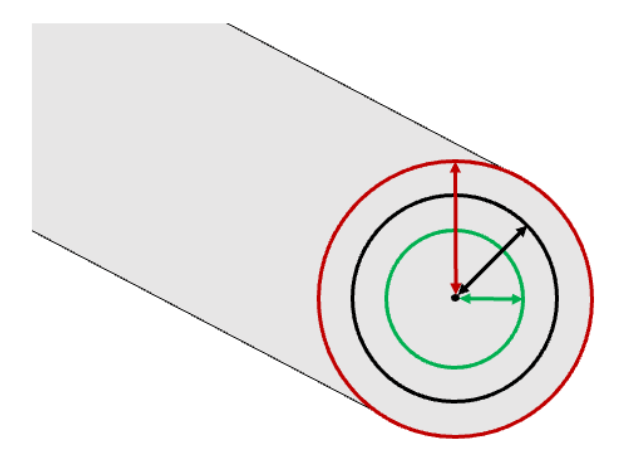


Figure 2 Schematic overview of the end of a bone pin with varying pin thickness. In red an increased pin radius is displayed, in green a decreased pin radius is displayed.

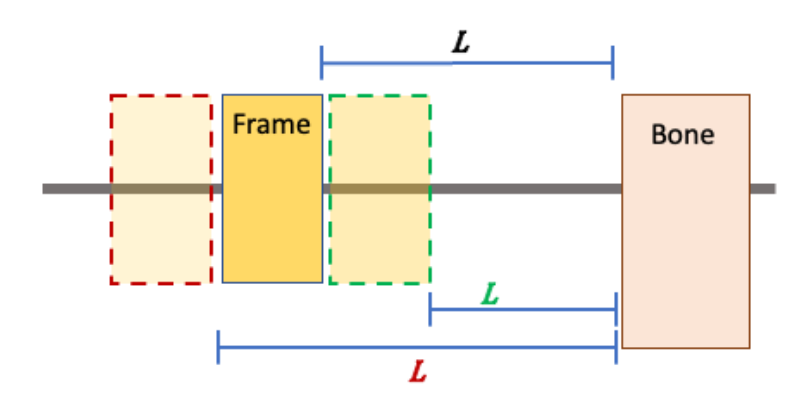


Figure 3 Schematic overview of the pin length adjustments. The red dashed block resembles a situation where the pin length is increased, the green dashed block resembles a situation where the pin length is decreased.







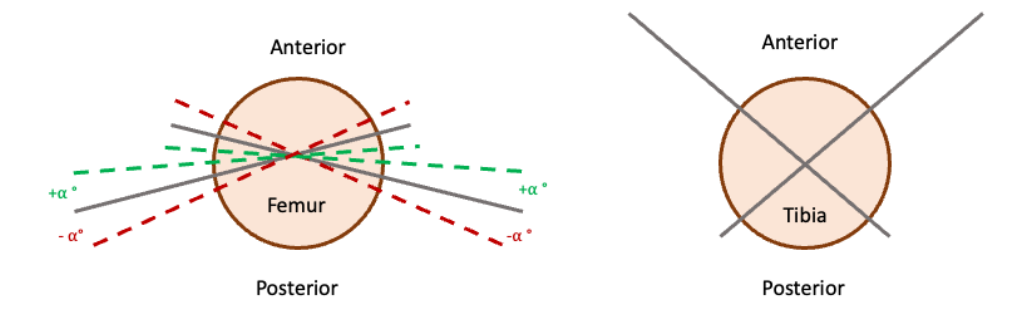


Figure 4 LEFT) Schematic top view of the femur bone with bone pin rotated in angle α (dashed green lines are rotated anterior, dashed red lines are rotated posterior). RIGHT) Top view of the tibia bone with bone pins. Tibia bone pins were not altered in this research.

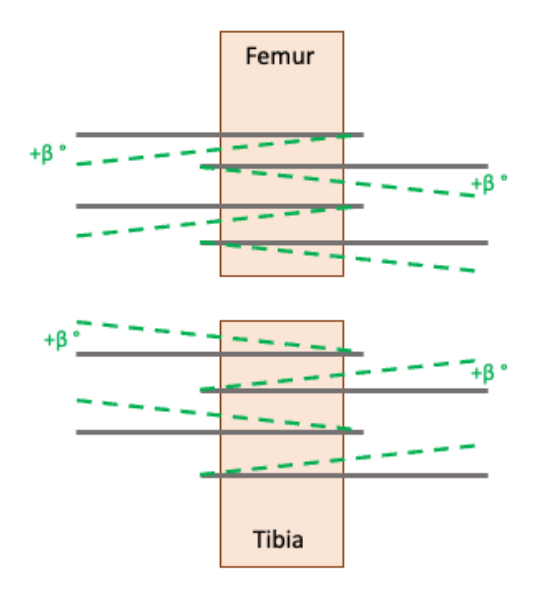


Figure 5 Schematic frontal view of the femur and tibia bones with bone pins. The green dashed lines are the conversion angles (β) that are adjusted in this research.

1.2 OBJECTIVES

- 1. To investigate the resulting JSW and relative knee joint rotations within in situ loading during KJD of the osteoarthritic knee.
- 2. To investigate the effect of pin thickness, pin insertion angles, and pin length on the mechanical behaviour of the ArthroSave frame and the resulting JSW of the osteoarthritic knee.
- 3. To investigate stress distribution of the femur and tibia bone at the bone-pin interactions.
- 4. To investigate the micromotions between the bone and individual pins.
- 5. To create relations between the JSW results of different FEM analyses that are modified with varying frame parameters.







2 BACKGROUND

2.1 SURGICAL PROCEDURE

2.1.1 PIN POSITION

The stainless-steel pins are placed during surgery, using the frame as a guide with sleeves to protect the surrounding soft tissue. The numbers (1-8) in Figure 6 visualizes the order of pin placement. The orientation of the pins is determined based on the leg morphology. The directions of the pins are based on the in safe angles in which no vital biological structures are damaged. For this reason, the femoral pins are inserted with an angle of 10 degrees posteriorly in the transversal plane (Figure 6, Panel 1, 2 and panel 5, 6). Tibial pins are inserted with an angle of 35 degrees anteriorly in the transversal plane (Figure 6 panel 3,4 and panel 7,8). There should be a gap of at least 15 mm between the skin and the block of the frame to compensate for the possible tissue swelling. These dimensions are aimed be kept constant during surgery for each patient. Nevertheless, in a surgical procedure, variation in placement is unavoidable (Wheeler et al., 2004).

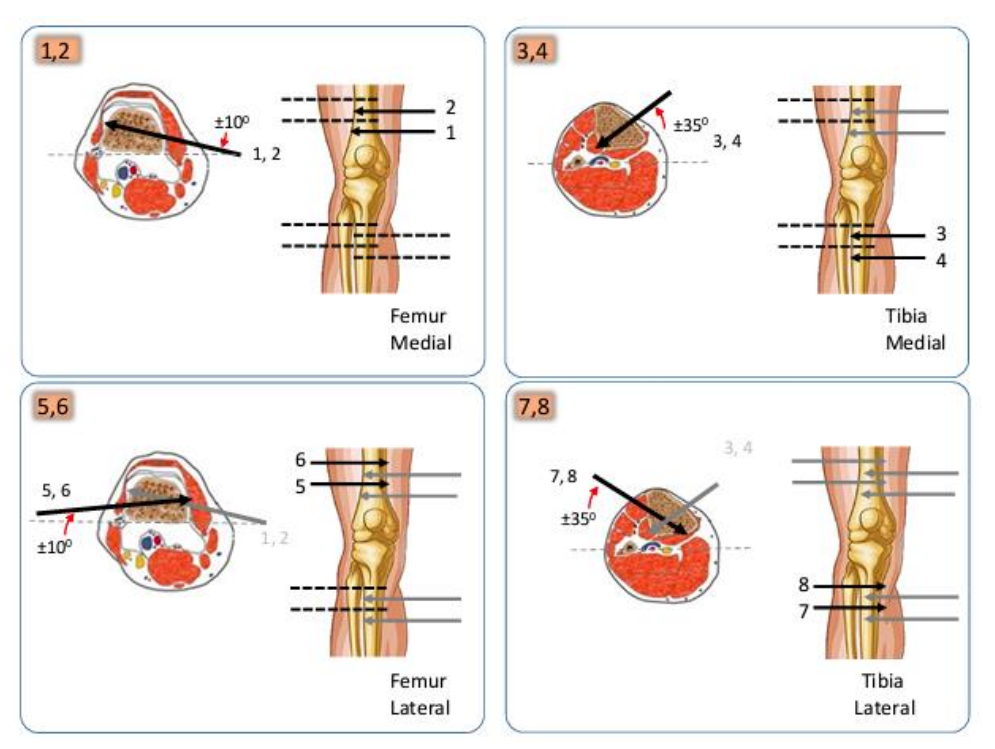


Figure 6 Overview of the positioning and order of the bone pin placement (ArthroSave, unknown).







2.1.2 PIN LENGTH

Pin lengths are an important factor in the functioning of the ArthroSave frame. Figure 7 displays a schematic overview of the pin length measurements. Figure 7 contains 5 measurements: The length of the clearance between skin and frame, the distance from the centre line of the bone to the centre line of the frame, the distance of bone drilled, the total pin length, and the effective pin length.

In the current research, the effective pin length, measured from the frame side of the cortical bone to the block of the fixator as visualized in Figure 7 was used for analysis. The results of the length measurements are listed in Table 1, which were based on data from 72 X-ray scans of patients undergoing distraction treatment in UMC Utrecht.

Table 1 Effective pin lengths and variability in pin lengths per pair of two pins

Pin	Effective pin length [mm]	
Medial femur	58.3 ±12.6	
Lateral femur	57.4 ±10.8	
Medial tibia	34.2 ±17.4	
Lateral tibia	50.6 ±16.2	

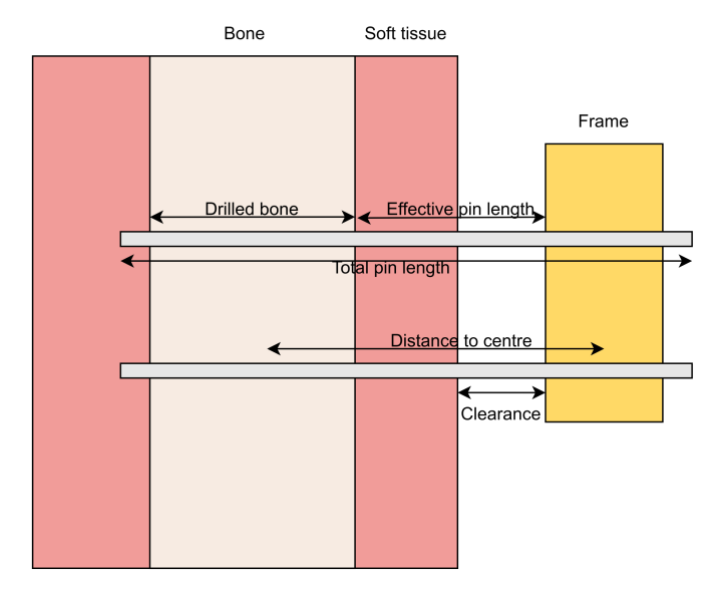


Figure 7 Schematic overview of pin dimensions with an external frame. The effective pin length is measured from the cortical bone to the medial side of the frame. There is a clearance of 15 mm secured during surgery.







2.2 THEORETICAL CALCULATIONS

2.2.1 THEORETICAL PIN DEFLECTION

The deflection of a pin could be calculated analytically using the Euler Bernoulli Beam Theory (Formula 1 and 2). These formulas assume that the pin is fully fixated on one end, consists of homogeneous material and of a consistent cylindrical shape (Timosjenko, 1953).

$$\delta = \frac{FL^3}{3EI} \tag{1}$$

and

$$I = \frac{\pi r^4}{4} \tag{2}$$

Where:

I = Area moment of inertia of the beam's cross-section in mm⁴
 (Describes the capacity of a cross-section to resist bending)

• **E** = Elastic modulus of the rod in MPa (N/mm²)

• **F** = Force acting on the tip of the rod in N

• L = Length of the rod in mm

• δ = Deflection of the tip of the rod in mm

• r = Radius of the rod in mm

Combining Equations 1 and 2 leads to Equation 3:

$$\delta = 4 \frac{FL^3}{3E\pi r^4} \tag{3}$$

Using Formula 3, the theoretical bending stiffness for multiple pin diameters (radius r) and lengths (L) can be calculated. The bending stiffness depends on pin radius to the fourth power and pin length to the third power.







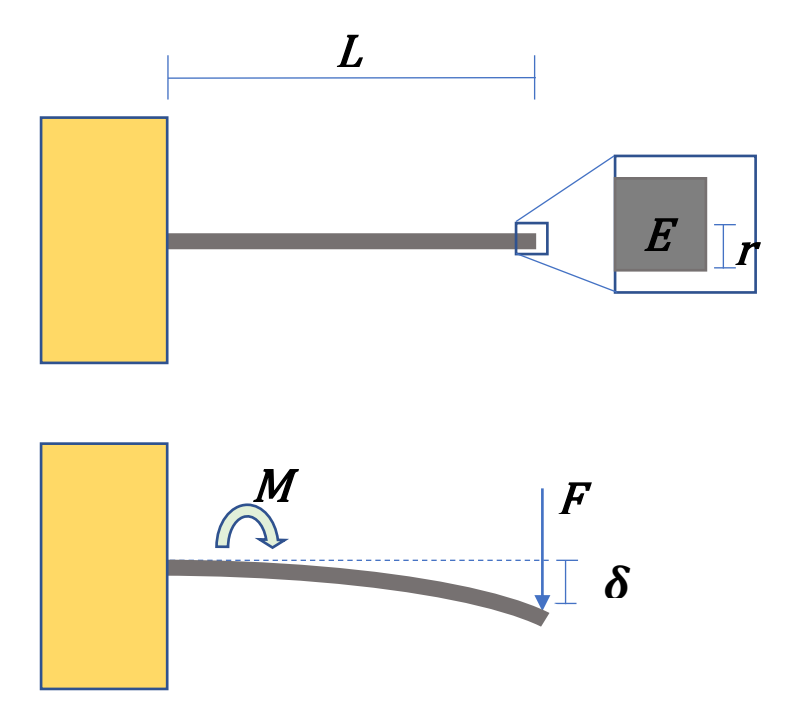


Figure 8 Schematic overview of the deformation of a pin that is completely fixated on the left side and free to move on the right side. L is the length of the pin, E is the elastic modulus of the material of the pin, r is the radius of the pin, F is the vertical force applied to the pin, M is the bending moment that occurs due to force F and δ is the displacement of the end of the pin.

2.2.2 THEORETICAL JSW DECREASE

Using theoretical bending calculations, the translation of the femur with respect to the tibia could be calculated. Therefore, a free body diagram of the simplified whole system is created (Figure 9). In this simplified system, the pin lengths are equal (50 mm), pin radius is 2,5 mm and the insertion angles are perpendicular to the bone surface. Also, complete fixation of the pins within the bone is assumed.

In case of a loading force of 1500 N applied vertically down on the femur, this force taken up by the bone pins ($F_{p1/4}$). For the simplicity of this example, the forces are equally divided over the four pins.

The force applied to one pin is thus:

$$F_{f1} = \frac{1}{4} * F_{applied} \tag{4}$$

Where:

• F_{f1} = The force in N applied to the first femoral pin

• $F_{applied}$ = The force applied to the femur

These forces are counteracted by a reaction force (- $F_{f_1/4}$) and a bending moment ($M_{f_1/4}$). This bending moment leads to a deformation of the femoral pins ($D_{f_1/4}$). The force than passes through the ArthroSave frame and is applied onto the tibia pins. This leads to a reaction force in the tibial pins. The reaction forces are still assumed to be proportional for simplicity. The tibial pins are then







exposed to a bending moment ($M_{t1/4}$) because the tibia is fixed. This bending moment leads to a deformation of the tibial pins ($D_{t1/4}$). Additionally, the JSW is decreased with an extra 3.2 mm due to the monotube spring deformation.

The total deformation of the femur with respect to the tibia is thus:

$$d_{JSW} = d_{f1} + d_{t1} + d_{spring} = 2 * d_{f1} + d_{spring}$$
 (5)

Where:

• d_{f1} = Deformation of the first femoral pin in mm

• d_{t1} = Deformation of the first tibial pin in mm

• d_{JSW} = Relative translation of the femur with respect to tibia (JWS decrease)

• d_{spring} = Deformation due to monotube spring

If these relations are substituted in the equation for a single pin (Equation 3) the following JSW decrease is found:

$$d_{JSW} = 2 * 4 * \frac{\frac{1}{4} * F_{applied} * L^{3}}{3 * E * \pi * r^{4}} + d_{spring} = 2 * \frac{4 * \frac{1}{4} * 1500 * 50^{3}}{3 * 198 * 10^{3} * 3.14 * 2.5^{4}} + 3.2 = 8.35 \ mm \tag{6}$$

Yet, while analysing the complete frame, the force might be distributed unevenly over the 8 pins. Pin lengths differ and angles of insertion could also play a role. Besides that, due to heterogeneity of the bone, the pins are not completely fixed and the load is not suspected to be fully concentrated. In Appendix Figure 5, alternatives methods for pin fixation are displayed. Concluding, theoretical beam deflections can give a rough simplified estimate, but will not provide a realistic approximation of the loading situation with the ArthroSave frame. Therefore, FEMs are used in the remaining part of this research.







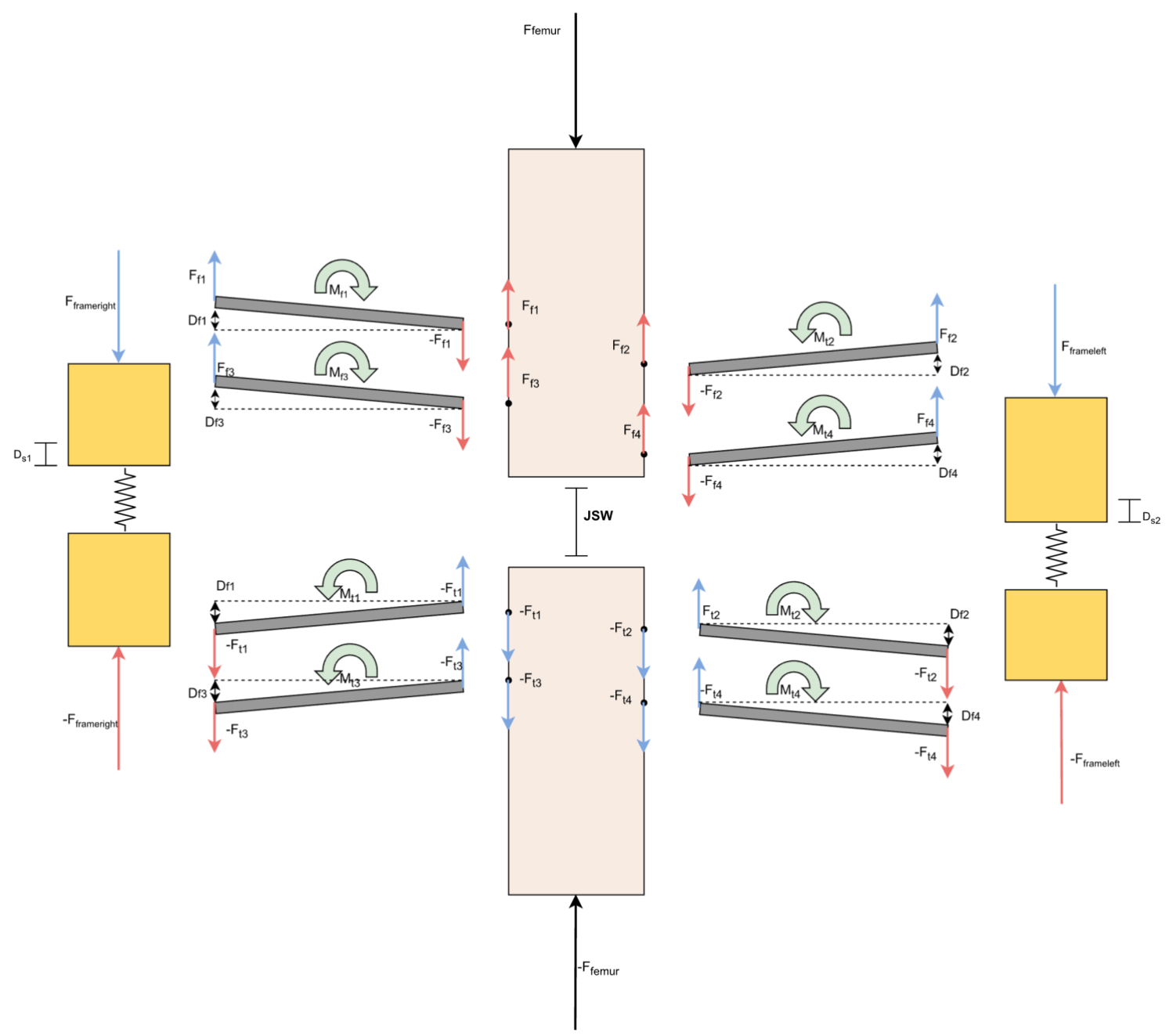


Figure 9 Free body diagram of the simplified external distraction frame used to perform theoretical JSW decrease calculation in a loading situation where the pins are completely fixed in the bone.







2.2.3 THEORETICAL PARAMETER ADJUSTMENTS

In the following examples, a cylinder is fully fixated on one side and free to move on the opposite side (as in Figure 8). In Figure 10 the stiffness of pins with three different diameters are plotted (4 mm, 5 mm, 6 mm). Stainless Steel (E=198*10³ MPa) pins with a length of 50 mm were used. Figure 11 displays the stiffness of pins with three different pin lengths (45 mm, 50 mm, 55 mm). Stainless Steel (E=198*10³ MPa) pins with a diameter of 5 mm were used in this figure. Based on this theoretical calculation, the effect of parameter adjustments is evident.

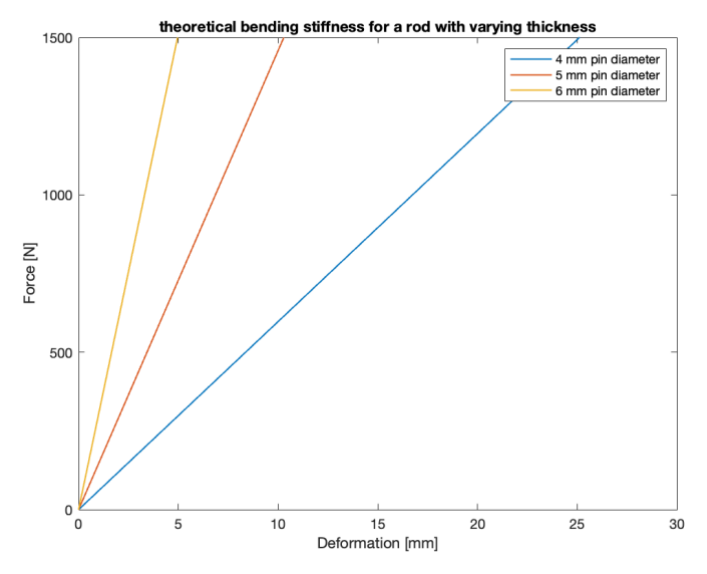


Figure 10 Theoretical bending stiffness of a single stainless-steel pin of 50 mm length based on diameter changes.

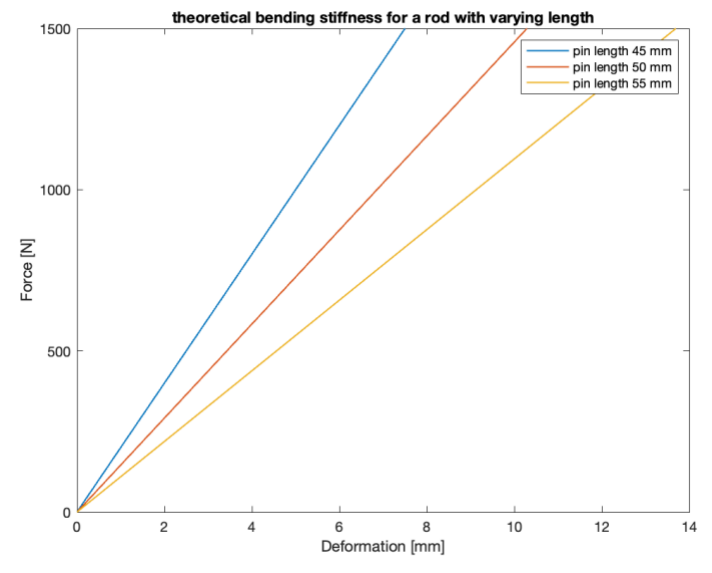


Figure 11 Theoretical bending stiffness of a single stainless-steel pin of 5 mm diameter based on length changes.







2.3 LOADING IN KJD TREATMENT

During KJD treatment, patients are asked to apply load on the treated knee by standing and walking. The force that is applied on the knee varies during a walking cycle. During normal walking, maximum loads are reached that exceed the body weight. Shelburne et al. (2005) estimated the femoral tibial forces to be up to 3 times body weight in a musculoskeletal simulation model. In prosthetic measurements performed by Taylor and Walker (2001), peak knee forces reported were 2.8 times body weight for walking, 2.8 times body weight for stair ascent, 3.1 times body weight for stair descent, and 3.6 times body weight for jogging. While research of Kutzner et al. (2010) found that average peak resultant forces were 2.6 times of the body weight during ground-level walking. During walking with crutches, however, peak forces are expected to be lower. Ground reaction force measurements by Stallard et al. (1980) found that around 1.3 times the body weight is carried by the affected leg when walking with crutches. Also, the body weight of the patient will influence the force applied on the knee. It is thus ambiguous how much force is exactly exerted on the effected knee during KJD. Therefore, in this research three examples of forces are highlighted:

- 1. Standing on both legs (0.5 times body weight)
- 2. Standing on the affected leg (1 times body weight)
- 3. Estimated peak force while walking with crutches (1.3 times body weight)







3 METHODS & MATERIALS

3.1 CREATION OF THE ORIGINAL MODEL

3.1.1 DATA DESCRIPTION

Data from the UMC Utrecht database was used to create the model.

Femur and Tibia bone were excluded from a full body CT scan from an anonymous female (77 yrs, 154 cm, 32.5 BMI). These bones were segmented in Materialize Mimics (Leuven, BE). This woman was diagnosed with OA KL grade 3 on the left knee (Kellgren and Lawrence, 1957). KL Grade 3 OA is sufficient to be eligible for KJD treatment. The CT scan was created in supine position. CAD data of the frame was provided by ArthroSave in a confidential fashion.

3.1.2 MODEL CREATION WORKFLOW

A 3D FEM of the ArthroSave frame, femoral, and tibial bones was created. All bone material was highlighted with bone Thresholding (Hounsfield Units (HU) 226-1686) in Mimics on the Dicom files. Slices above the femur and below the tibia were removed. Multiple slice edit tool was used to remove the knee cap. The split mask tool was used to separate the femur and tibia bones. Then, the 3D parts were created in Mimics and exported to Materialise 3-Matic.

In 3-Matic, the bones were post-processed. Bone pins were created as cylinders with dimensions length 200 mm and diameter 5 mm. The pins were moved towards the right position using the angles in Figure 4 and 5. Consequently, the ArthroSave frame parts were orientated to match the average pin lengths in Table 1. The femur was then translated in axial direction to replicate a distraction of 5 mm. Bone holes were created by subtracting the geometries of the pins from the bone geometries.

Volumetric mesh was created with adaptive mesh size depending on the pin position (Subsection 3.1.3). The assembly was exported back to Mimics where material properties were assigned to the bones based on HU (Subsection 3.1.4). The assembly including material properties was then exported to Abaqus FEA. In Abaqus, first, material properties of the frame and pin parts were assigned. Consequently, connection between parts was set (Subsection Pin-Bone Connection). Then, loads and boundary conditions were applied (Subsections Boundary Conditions and Loading Conditions). Schematic overview of the complete workflow is visualized in Figure 12. Also, stepwise model creation is added in the Appendix. This resulted in the 3D model assembly and the 3D FEM in Figure 13.







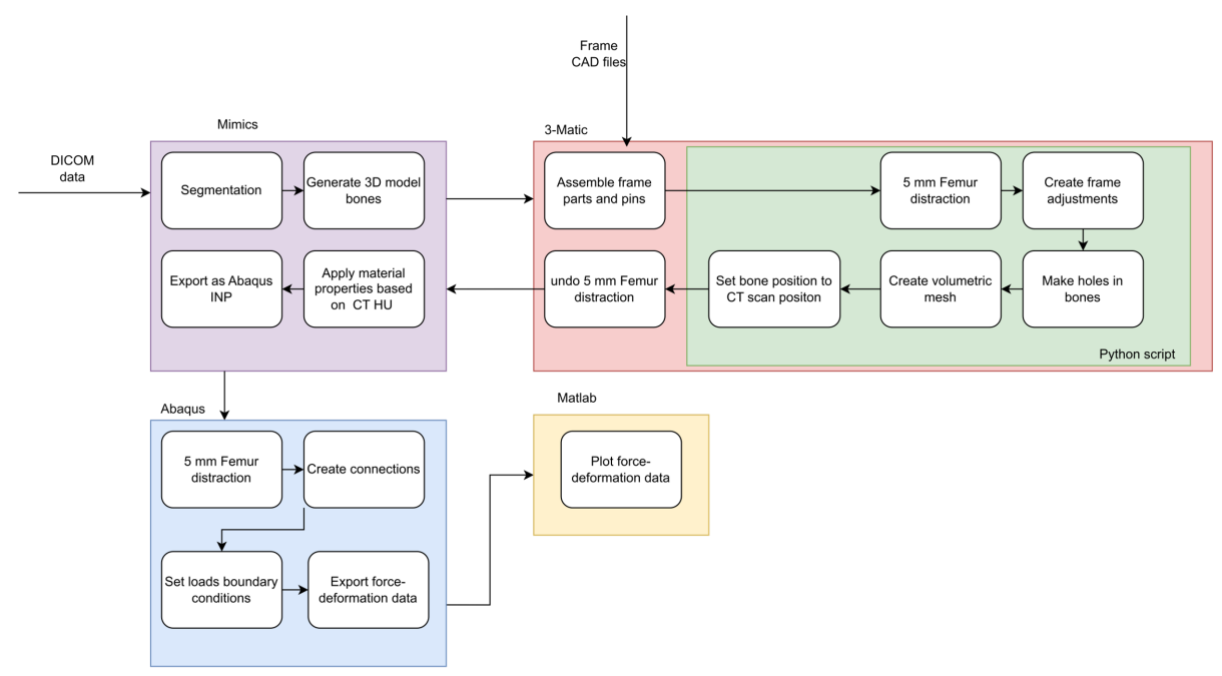


Figure 12 Flowchart of the development process of the KJD finite element model and results. Each block resembles a required operation to generate the FEM. The colours resemble different software programs in which the operations are performed (purple = Mimics, Red = 3-Matic, Green = Python, Blue = Abaqus, Yellow = Matlab).

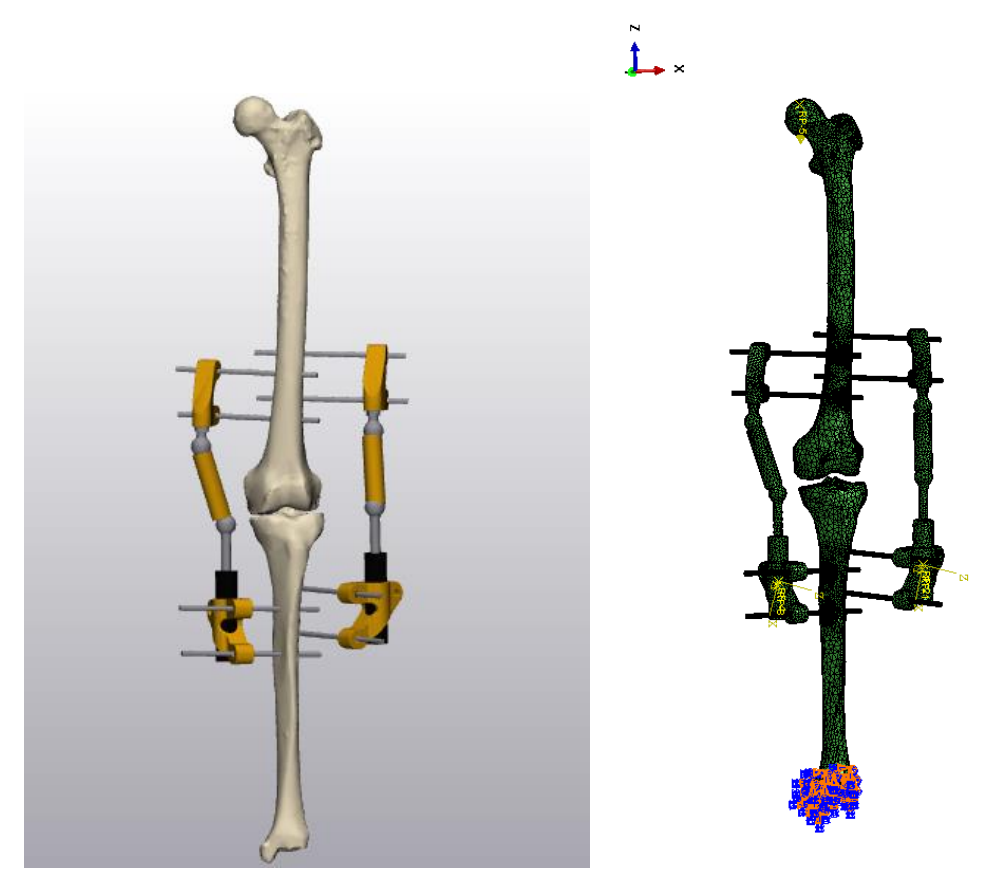


Figure 13 LEFT) Picture of the ArthroSave model assembly attached to the femur and tibia bone. RIGHT) FEM of the ArthroSave frame connected to the femur and tibia bone. Including boundary condition at the distal tibia and loading force at the proximal femur.







3.1.3 DISTRACTION

A distraction distance of 5 mm is sufficient for effective treatment (Jansen, Mastbergen, et al., 2020). This is typically performed in a step-by-step process where the knee is distracted by 2 mm during surgery and for three consecutive days 1 mm daily. In the model, the femoral bone was translated 5 mm along the longitudinal (z) axis to resemble a KJD situation (Figure 14). The femoral bone was translated, put back in its original position, and then translated again. This was required because the Hounsfield units corresponded with the spatial location of the CT scan. The holes and mesh were generated in the distracted position. After that, the material assignment was performed in the original position. Lastly, in Abaqus, the distracted position was used to connect the pins in the holes.

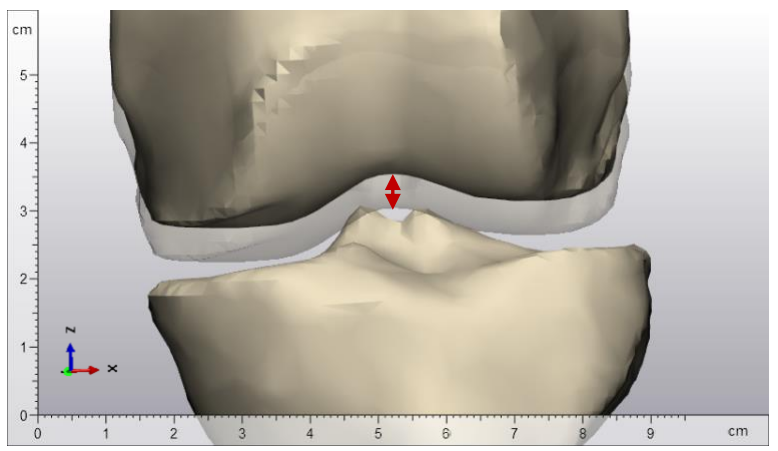


Figure 14 Picture of the JSW of the knee joint. The red arrow shows the applied distraction of $5\,\mathrm{mm}$ which is performed in KJD treatment.







3.1.4 MESH CONVERGENCE

Meshing is important in FEM of biological tissues (Hölzer et al., 2013). Usually, there is a trade-off between the accuracy of the model and the computational time. To optimize the balance between computational time and model accuracy, a mesh convergence study was performed. This was performed with a simplified model build with a block and pin (Figure 15). Considering the expected large deformation within the bone pins, seed lengths were altered for the pin. Results of the mesh convergence study are plotted in Figure 16. The bending results of the mesh convergence are close to the theoretical calculations of pin bending (difference < 1 mm).

Initially, pin seed lengths of 4 mm were used. In increment steps of 0.5 mm the seed length was reduced. For a seed length of 2 mm, the deformation reached a constant value. Therefore, a maximal seed length of 2 mm was used for the complete bone model. Also, an adaptive mesh was generated depending on the region of interest. This resulted in a smaller mesh size around the bone-pin interaction, which increases the accuracy in this region. This resulted in a model with a total of 764087 Tetrahedral elements. TET10 elements were used in the FEM experiments.

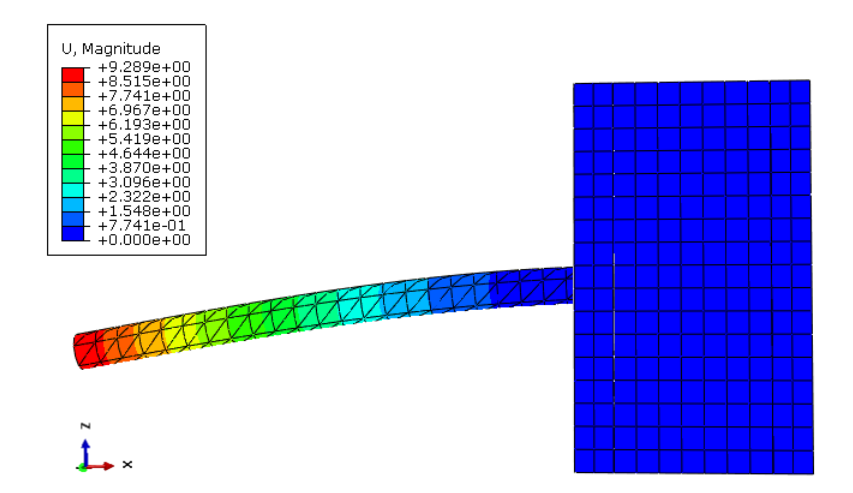


Figure 15 Example model that is used to determine the mesh seed length. The colour of each element resembles the elements' deformation (z-axis). The deformation for the mesh convergence was measured at the tip of the pin.







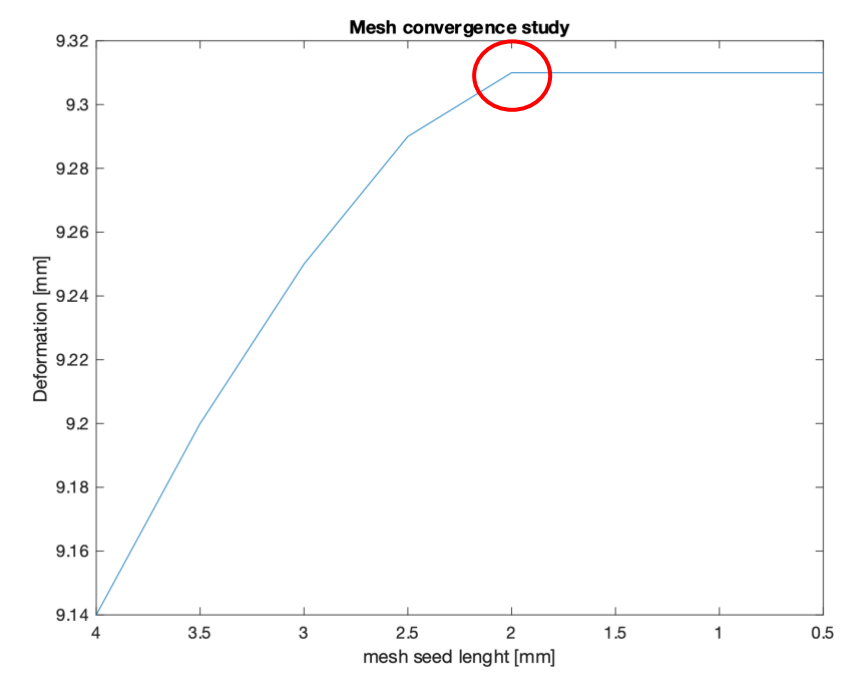


Figure 16 Shows the deformation of the tip of the pin in the test model for various mesh seed lengths. Mesh convergence is observed from 2 mm seed length (red circle) and smaller.

3.1.5 MATERIAL ASSIGNMENT

A total of 10 material types per bone were used to cover the trabecular and cortical bone. The grey value-based method was used to transform Hounsfield Units into bone density values. Elastic properties were assigned using a quadratic formula (Equation 7). Poisson's ratio (v) had a constant value of 0.3.

$$E = 0.004 * p^{2.01} \tag{7}$$

Where:

- **E** = Elastic modulus of the bone [MPa]
- $p = \text{Bone density } [g/\text{mm}^3]$. Determined with CT Hounsfield units with HU range = [50 1900]

This resulted in 10 heterogeneously distributed bone materials as shown in Tables 2 and 3. The elastic modulus (E) ranged from 10.4 MPa for the trabecular bone to 17,748 MPa for the cortical bone. The density had a cut-off value of 50 mg/cm³ to prevent negative density values.







Table 2 Material properties of the femur bone in the finite element model

Material name	Density p [mg/cm ³]	Elastic modulus E [MPa]	Poisson's ratio v
femur 0	50.0	10.4	0.3
femur 1	155.2	101.4	0.3
femur 2	363.3	560.1	0.3
femur 3	571.4	1391.6	0.3
femur 4	779.4	2597.4	0.3
femur 5	987.5	4179.0	0.3
femur 6	1195.5	6137.1	0.3
femur 7	1403.6	8472.6	0.3
femur 8	1611.7	11186.0	0.3
femur 9	1819.7	14277.9	0.3
femur 10	2027.8	17748.6	0.3

Table 3 Material properties of the tibia bone in the finite element model

Material name	Density p [mg/cm ³]	Elastic modulus E [MPa]	Poisson's ratio v
tibia 0	50	10.4	0.3
tibia 1	153.5	99.1	0.3
tibia 2	358.0	543.7	0.3
tibia 3	562.5	1348.3	0.3
tibia 4	767.0	2514.7	0.3
tibia 5	971.5	4044.1	0.3
tibia 6	1176.0	5937.2	0.3
tibia 7	1380.5	8194.8	0.3
tibia 8	1585.0	10817.4	0.3
tibia 9	1789.5	13805.6	0.3
tibia 10	1994.0	17159.9	0.3

Homogeneously distributed stainless Steel (E = $198*10^3$ MPa, v = 0.3) was assigned to the pins and the frame parts. This material is used in the ArthroSave frame as described in Section **Error! Reference source not found.**. Linear material properties and linear geometries are used in this FEM model.

3.1.6 PIN-BONE CONNECTION

Rigid fixation between bone and pins is found to be one of the likely sources of error in FEM fixators (Drijber et al., 1992). This study also tested the differences between compressive (Figure 17) and compressive – tensile (Figure 18) fixation methods for the bone pin interaction. There was a significant difference of 16% stiffness decrease in the compressive fixation method. Results of these tests are displayed in the Appendix Figure 1.

Within the 6 weeks KJD treatment procedure there is no osseointegration expected between the bone and the uncoated bone pins (Albrektsson and Johansson, 2001). Therefore, no tensile forces are believed to be exerted at the bone-pin interfaces. Hence, a solely compressive method has been used to model the bone pin interaction. This method allows micromotions to occur in the FEM analysis. To realize this interaction without computational difficulties, the pins and bone were only fixed at locations where compressive forces were expected (Figure 19).







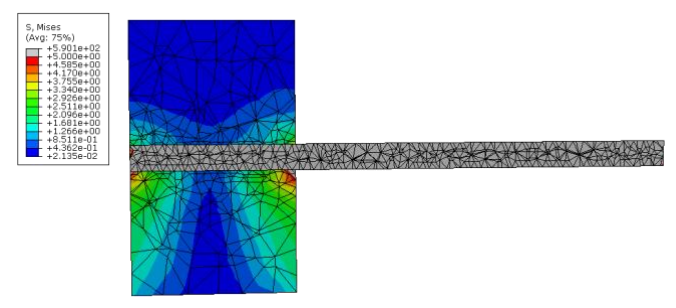


Figure 17 Example: Stress distribution in a bone pin interaction during pin loading with completely fixated pins that are subjected to tensile and compressive stresses

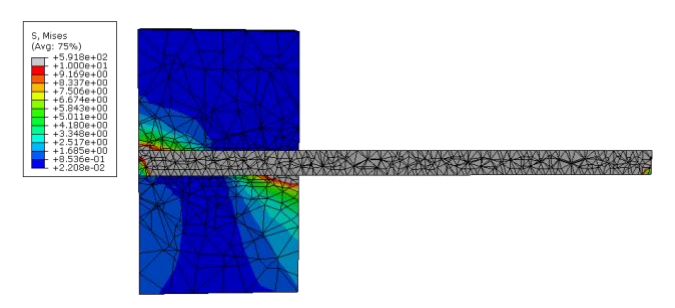


Figure 18 Example: Stress distribution in a bone pin interaction during pin loading with partly fixated pins that are only subjected to compressive stresses

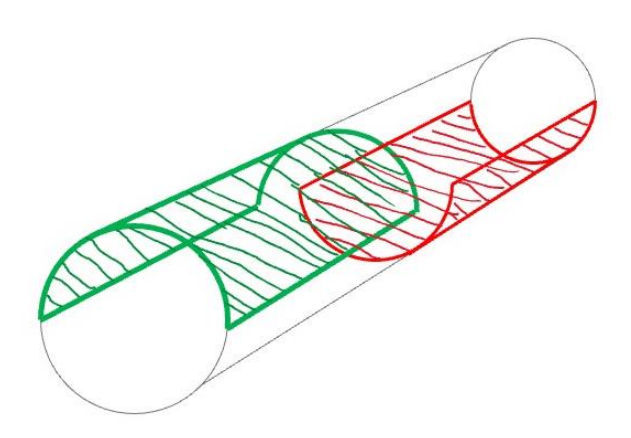


Figure 19 Schematic cross section of the pin part that is fixed in the bone. The colors (red lateral, green medial) represent the places where the pins were fixated. On these places, compressive forces are expected while loading from the lateral side.

3.1.7 MONOTUBE SPRING MODELING

The monotubes were modelled using a non-linear spring in Abaqus. Two connector points for the spring were selected and the properties are described in Table 4. These numbers result from a single spring with a stiffness of 144 N/mm and a maximal displacement of 3.2 mm. The maximal displacement was realized by introducing a high reaction force for a deformation smaller than -3.2 mm. For a loading force of 460.8 N, one spring would be maximally compressed. Considering there are two parallel positioned springs, these springs are expected to maximally compress around a loading force of 921.6 N.







Table 4 Mechanical properties of the springs within the monotubes of the frame. Each spring will act as completely stiff (exerting $1000000~\rm N$) after a deformation of $3.2~\rm mm$.

Deformation [mm]	Spring force [N]
-3.201	-1000000
-3.2	-460.8
-1	-144
0	0
1	144

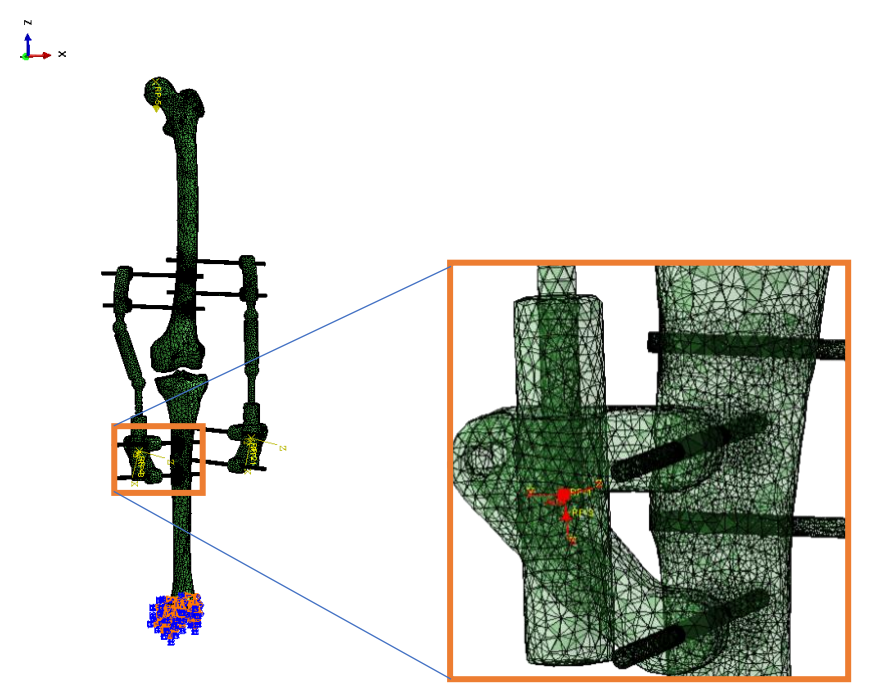


Figure 20 Enlarged picture of the spring positioning within the monotubes in the FEM. Springs are applied on both sides of the frame. The elements are opaque in this picture to see though them.

3.1.8 BOUNDARY CONDITIONS

Boundary conditions should be applied to the model to keep the system stable when loaded (Figure 21). The bottom nodes of the tibia were fixed as a boundary condition to represent the normal force that was applied by the talus and calcaneus bone. This boundary condition prevented translations in the x-, y-, and z-directions and rotations in the x-,y- and z-directions.

To allow for free movement of the JSW, there was no boundary condition applied within the joint.







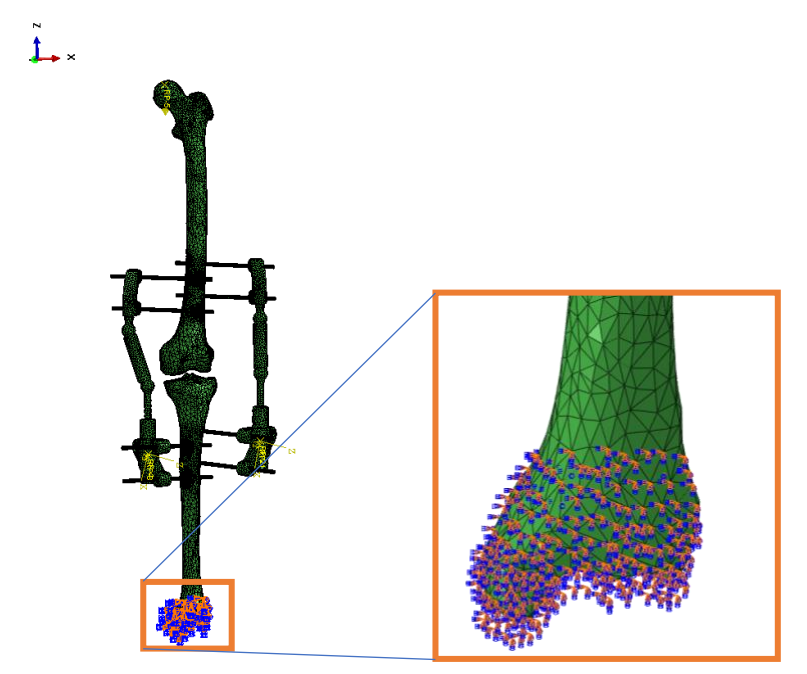


Figure 21 Enlarged picture of the boundary condition placement within the FEM. Bottom nodes are constraint to move in all translational and rotational directions.

3.1.9 LOADING CONDITIONS

To examine the full behaviour of the frame, a relatively high load of 1500 N was applied. This load was much larger than the patient's body weight. This way, the point of JSW closure can be determined. The whole spectrum of loading was thus explored, and the Force-Deformation graph was plotted in the Chapter Results. The resulting deformation for a specific force can be deducted from the graph, taking the linearity of the FEM into account.

The load was a concentrated force that was applied on a reference point tied to the upper surface of the femoral head. This force pointed purely in the z-direction, parallel to the femoral bone as shown in Figure 22.

Three examples of forces are highlighted in the results. These forces are created based on the scaling factors from Section Loading in KJD treatment and the body weight of the patient from the CT scan (77 kg).







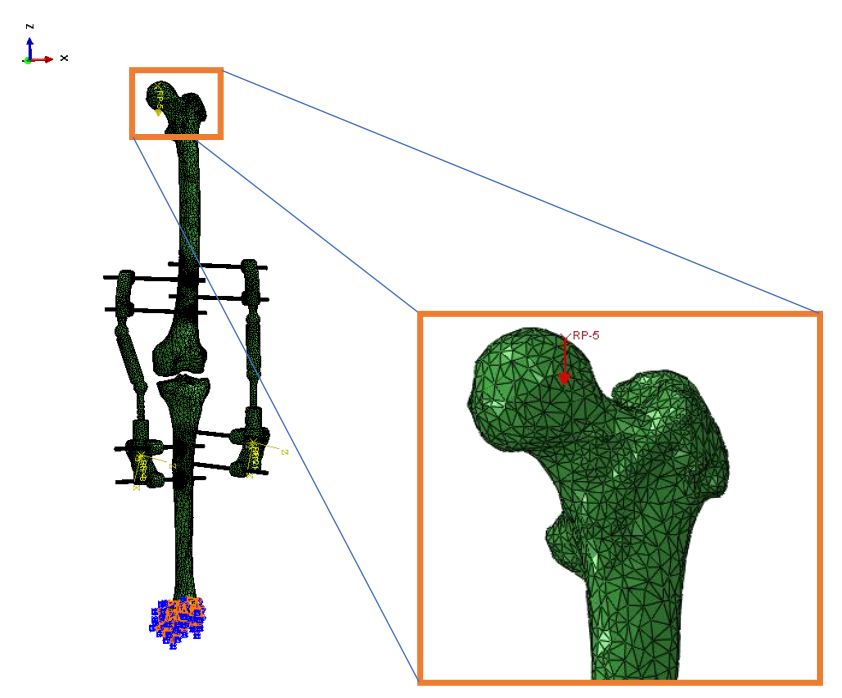


Figure 22 Expansion of the loading condition within the FE model. A load of 1500 N is applied to a reference point which is connected to the surface of the femoral head.







3.1.10 JSW AND ROTATION CALCULATION

In this research, the region of interest was the JSW. Therefore, the distal femur and proximal tibia were measured (point 3 and 4 in Figure 23). Points 1 and 2 were used to apply the load and boundary condition respectively. To obtain the JSW decrease during loading, the displacement of the distal femur was subtracted from the displacement of the proximal tibia.

The rotations of the distal femur and the proximal tibia were calculated for 1500 N. The proximal tibia rotations were subtracted from the distal femur rotations to obtain the relative rotations within the JSW. Rotations could occur in 3 different directions. The investigated rotations are displayed in Figure 24.

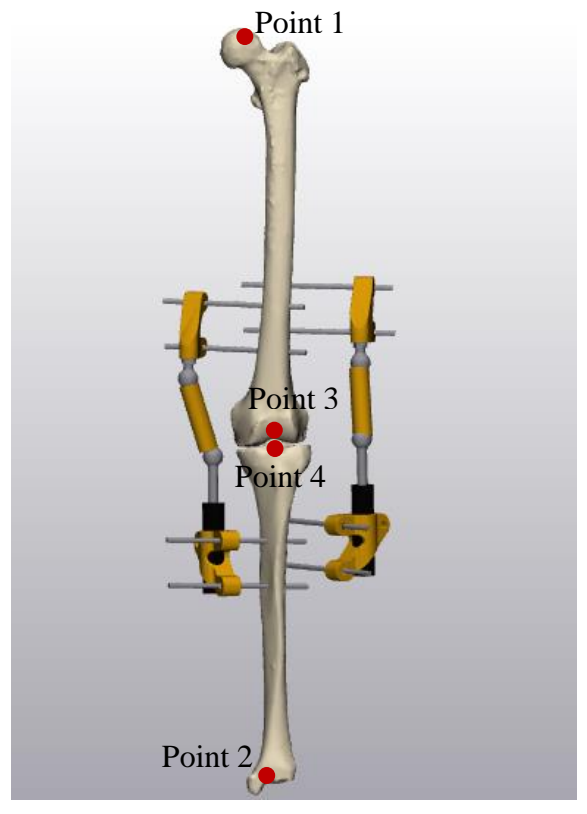


Figure 23 Picture of the 3D model of the KJD frame and the deformation measurement locations: 1 proximal femur, 2 distal tibia, 3 distal femur, 4 proximal tibia.







	Positive angle	Neutral angle	Negative angle
		# DEVISOR	HPKKNN
x angle			
	Flexion		Extension
y angle		i.	L.
	Adduction		Abduction
z angle			
	Exorotation		Endorotation

Figure 24 Possible relative rotations within the knee joint. The red arrows display the rotation that is shown in each picture.

3.1.11 JOINT SPACE WIDTH DETERMINATION

Since the articular surface is a 3D landscape, the JSW was not one value but can be calculated on multiple positions. To work with this JSW value, multiple points were created on the articular surface, and minimum and mean values were calculated. These measurements were performed in Materialise 3-matic. Results of these measurements are found in Section 4.2 in Chapter Results. The minimum pre-treatment JSW was used as criteria measure such that across the models created later, the following assumptions are made:

- JSW was increased by 5 mm after distraction with respect to initial minimal JSW.
- The difference between the deformation of the distal end of the femur and the proximal end
 of the tibia leaded to an equal decrease in the JSW.







3.2 FRAME ADJUSTMENTS

3.2.1 ADJUSTED PIN THICKNESS

The standard diameter of the pins used during KJD is 5 mm (Jansen, Mastbergen, et al., 2020). Variations have been applied by changing the pin diameter in a range between 4 and 6 mm (Figure 25).

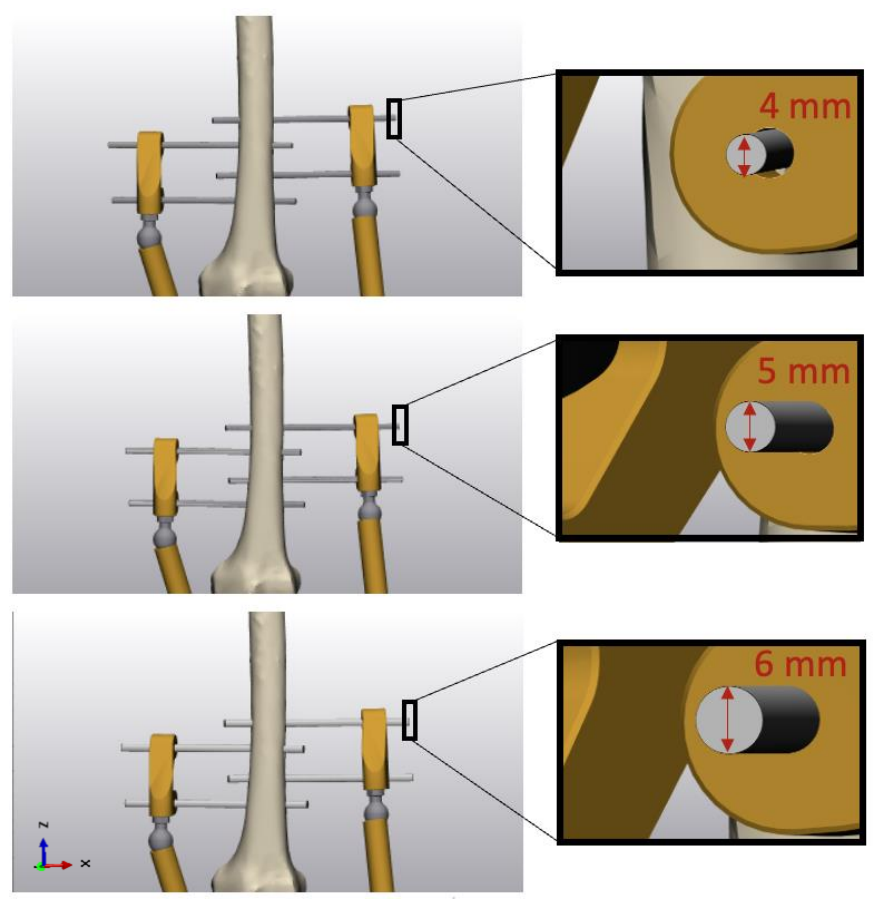


Figure 25 Pictures of the pin diameter adjustments. Enlarged pictures are shown on the right where pin diameters are 4,5 and 6 mm respectively. The red arrow explains the diameter of the pins from a side view.







3.2.2 ADJUSTED EFFECTIVE PIN LENGTH

The length of the pins used in the external fixation depends on the patient's morphology. Average pin lengths measured on knee X-rays in treated patients are listed in Table 1 in Chapter Background. In this research, variations were applied from -10 mm to + 10 mm with respect to the average pin lengths. The frame parts were reoriented to connect the distraction frame.

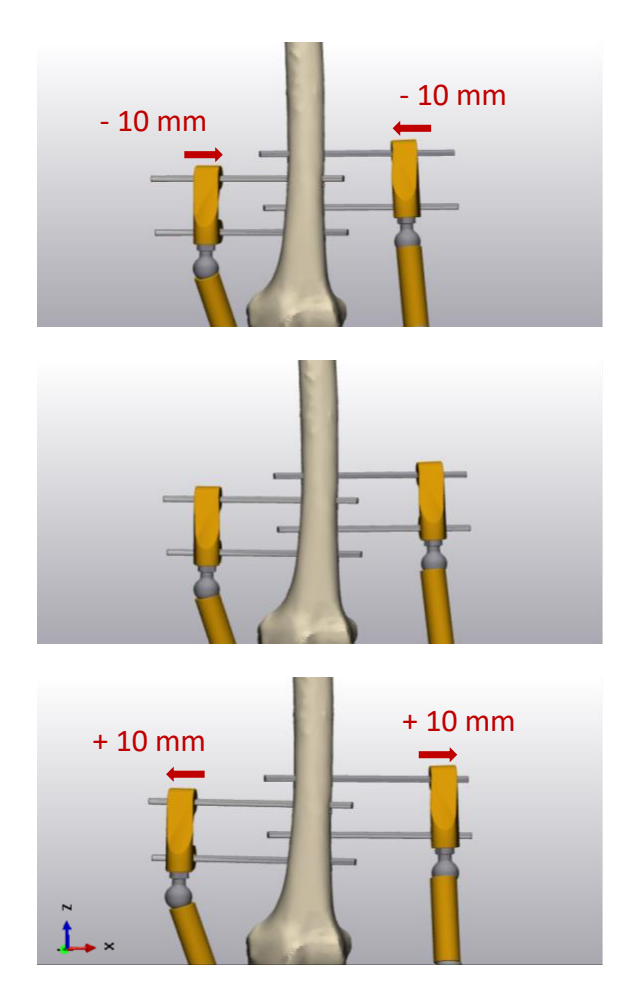


Figure 26 Pictures of the pin length adjustments. The lengths of all pins are 10 mm longer at the top picture, unadjusted in the middle picture and 10 mm shorter in the bottom picture with respect to the average pin lengths.







3.2.3 CONVERGING PINS

Pins were rotated around the Y-axis to create converging pins assemblies, for both the tibial and femoral pins (Figure 27). This was done in conversion angles of 5 degrees and 10 degrees.

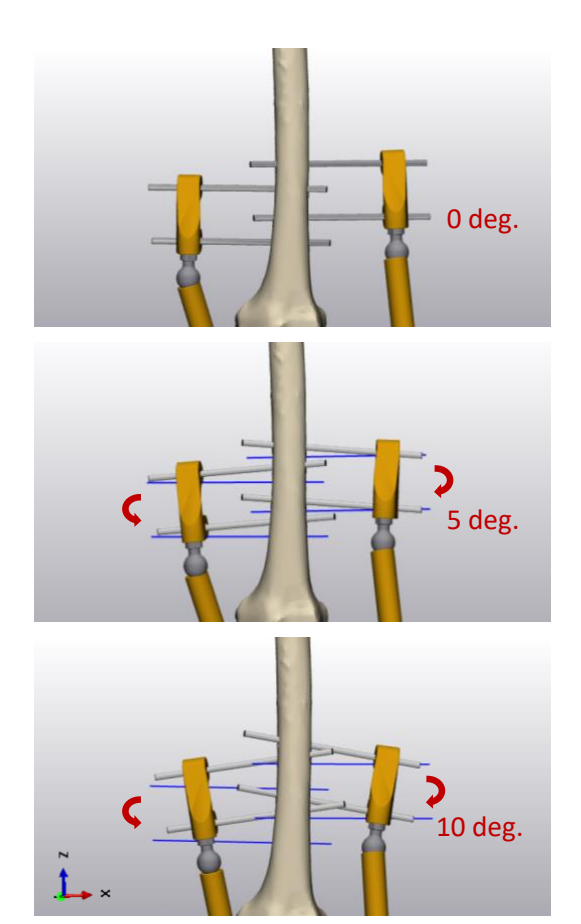


Figure 27 Picture of the conversion angle adjustment. The conversion angle in the top picture is unaltered, in the middle picture 5 degrees conversion is applied and in the bottom picture 10 deg conversion is applied. The blue lines resemble the original pin insertion angles.







3.2.4 ROTATED PINS

Changing the insertion angles was performed in step 16 in Workflow. The rotated pin principle was a rotation round the longitudinal axis (z-axis). The rotated pins are displayed in Figure 28. The angle of the femoral half pins was changed by +10 and -10 degrees with respect to the angles described in Chapter Background.

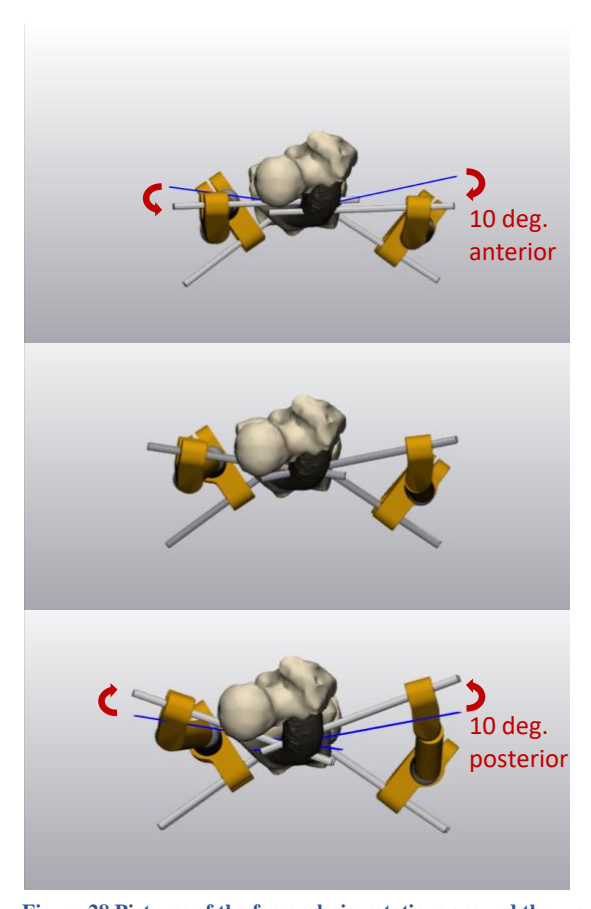


Figure 28 Pictures of the femoral pin rotations around the y-axis. Femoral pins are rotated 10 degrees anterior in the top picture, no adjustment is made in the middle picture and the pins are rotated 10 degrees posterior in the bottom picture. The blue lines resemble the original pin positions.







3.3 INDIVIDUAL PIN DIFFERENCES

3.3.1 STRESS CONCENTRATIONS

The stress concentrations were visually compared using results from the ABAQUS viewport. For each pin the maximal principal stress components were examined and reported. Also, the max principal stress location of the Femur and Tibia bone were reported.

3.3.2 MICROMOTIONS

Two points were measured for each bone-pin interaction to calculate the micromotions between bone and pin. The measurement points on the femoral pins were located on the top side of the pins. For the tibial pins, the measurement points were located on the bottom side. This was chosen because of the direction of pin deformation (top pins bend up, bottom pins bend down). The absolute distance between the node on the pin and the node on the bone was calculated using the Pythagoras Theorem (Equation 8):

$$d_{micro} = \sqrt{(x^2 - x^1)^2 + (y^2 - y^1)^2 + (z^2 - z^1)^2}$$
 (8)

Where:

- Point 1 has coordinates (x1, y1, z1)
- Point 2 has coordinates (x2, y2, z2)

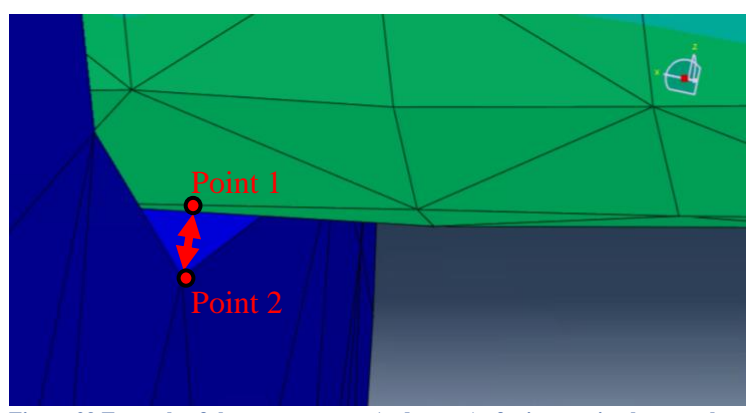


Figure 29 Example of the measurement (red arrow) of micromotion between bone (blue) and bone pin (green) at the bone pin interaction within the FEM.







3.4 RELATIONS FRAME PARAMETERS

The FEMs created in this research can be used to define a relation between the JSW decrease of the knee-reviver and frame parameters as pin diameter and length. To create this relation, stiffnesses for different configurations were created. An important note is that the stiffness was calculated for 1500 N. Stiffness must be defined for a specific force due to the monotube springs that cause a nonlinear JSW decrease. In addition to the configuration created in Section Frame Adjustments, two extra configurations were created for both pin diameter and, resulting in 5 FEMs per parameter. Respectively, multiple different types of relations could be proposed. This research was limited to 3 different types of relation. These relations are a 1st-order polynomial (linear), 2nd-order polynomial (quadratic), and 3rd-order polynomial (Cubic).

The following relations are proposed for diameter:

Sd = g * D + hLinear:

 $Sd = g * D^2 + h * D + i$ Quadratic:

 $Sd = g * D^3 + h * D^2 + i * D + i$ Cubic:

Where, Stiffness (Sd) is dependent on diameter (D) and fitting parameters (g, h, I, j).

And for length:

Linear: Sl = a * L + b

Quadratic:

 $Sl = a * L^{2} + b * L + c$ $Sl = a * L^{3} + b * L^{2} + c * L + f$ Cubic:

Where, Stiffness (SI) is dependent on length (L) and fitting parameters (a, b, c, f).

The stiffness difference (error value) between each datapoint and the fitted relation resulted from the Polyfit algorithm. Mean error values were calculated by averaging over the error values. These mean error values were used as the criterium to select a polynomial relation in Chapter Results.







4 RESULTS

4.1 VALIDATION

Model validation was performed using a dataset from a real-world experiment carried out by BAAT medical (Hengelo, Netherlands). This experiment consisted of an axial stiffness test of the ArthroSave frame connected to two polyethylene (PE) blocks resembling the Femur and Tibia.

To replicate this test, a validation FEM was created in Abaqus which had a comparable geometry (Figure 30). Results of the real-world experiment compared to the validation FEM were displayed in Figure 31. The experimental stiffness lines were derived from BAAT experimental data (Appendix Figures 2, 3 and 4). The stiffness of the validation FEM corresponded with the average experimental stiffness with a difference of -0.91 percent for a force of 1100 N.

The validation model thus corresponded with the real-world experiment. In the model of the knee joint used in this research, the same mesh, material properties, boundary conditions, and loading conditions were used. Therefore, it was assumed that the stiffness of the knee joint FEM will correspond with a real set-up of the ArthroSave frame attached to two bones.

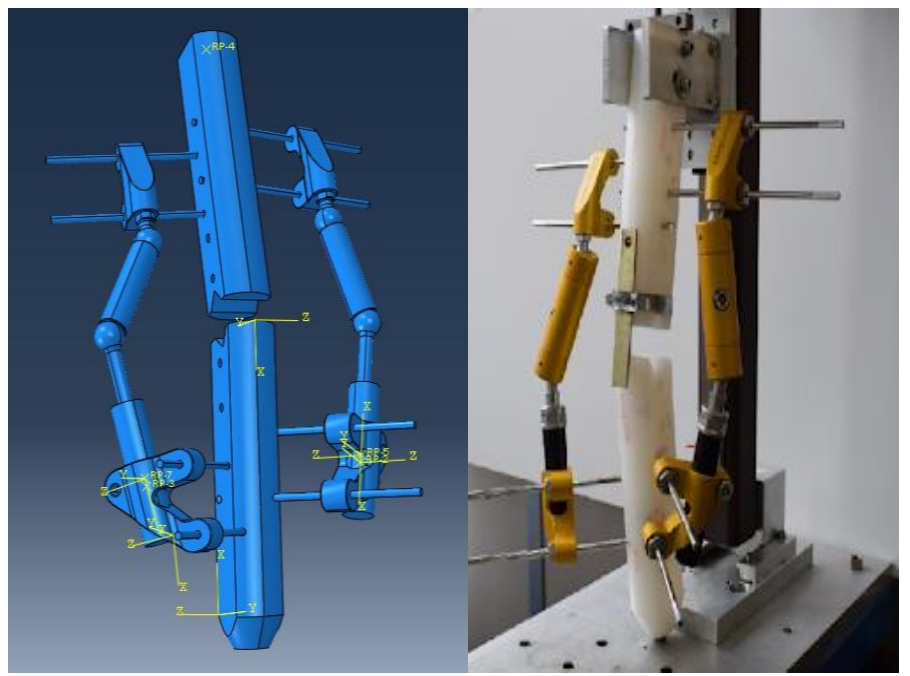


Figure 30 LEFT) Picture of the PE FEM used to replicate the BAAT experimental tests. RIGHT) Picture of the BAAT experimental axial loading test set-up.







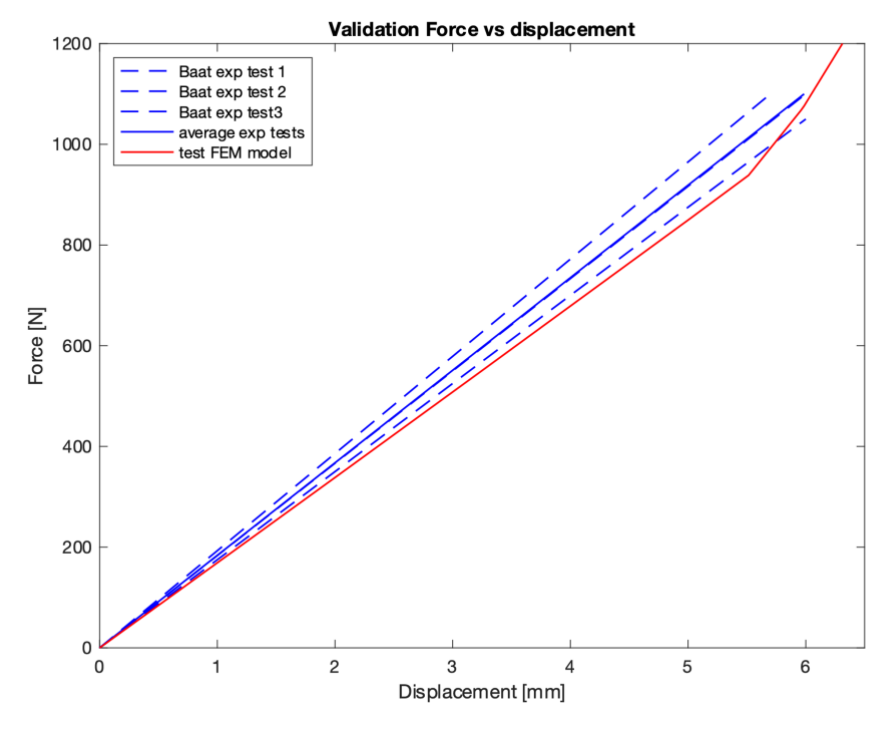


Figure 31 Force-Displacement graph comparing the BAAT experimental results with the PE FEM. Exp test 1-3 resemble the three consecutive tests that have been performed in the BAAT experiment (dashed blue lines). A different of -0.91 percent stiffness is observed for a loading force of 1100 N between the FEM (red line) and the average of the experimental tests (continuous blue line).

4.2 JSW MEASUREMENTS

In the OA knee that was used in the current research, the minimum JSW was 2.20 mm, measured on the lateral compartment of the knee. The mean JSW was 3,68 mm, measured in both the medial and lateral compartment. In the remaining part of the results, the initial JSW will be indicated as one number with a value of 2.20 mm. During KJD treatment this value is enlarged to 7.20 mm.

Table 5 Distances within the JSW for multiple locations before and after KDJ

	Location	JSW Distance [mm]
Before KJD		
	Lateral anterior	5.14
	Media anterior	5.10
	Lateral	3.39
	Medial	2.51
	Lateral posterior	2.20
	Medial posterior	3.37
	Minimum	2.20
	Mean	3.68
After KJD		
	Minimum	7.20
	Mean	8.68







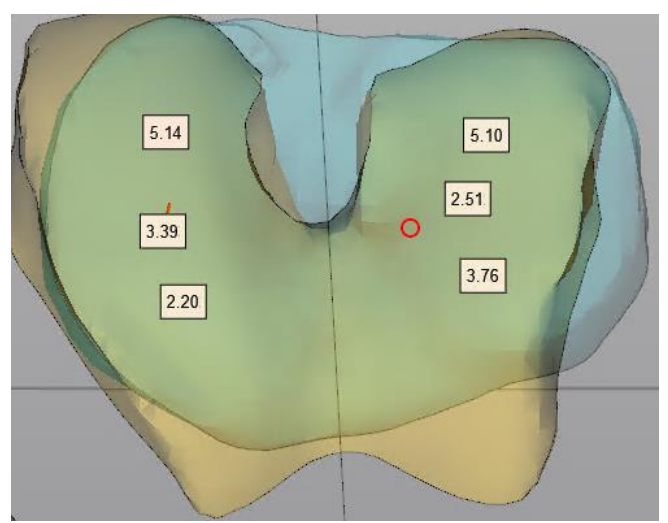


Figure 32 Top view of the femur bone (yellow) and tibia bone (blue) and the locations and values of the JSW measurements before KJD. Minimum JSW was 2.20 mm, measured at the lateral posterior compartment.

4.3 JSW DECREASE

The JSW decrease in vertical z-direction is shown in Table 6. The differences between the femoral head and the distal femur can be perceived as femoral bending. The tibial bending equals the displacement of the proximal tibia.

 $\underline{Table\ 6\ Displacement\ of\ the\ distal\ femur,\ proximal\ tibia\ and\ JSW\ in\ vertical\ (z)\ direction\ for\ a\ load\ of\ 1500\ N}$

Model	· ·		JSW decrease [mm]
	femur [mm]	proximal tibia [mm]	
Original set-up	6.635	0.069	6.566
Conversion 5 deg	6.839	0.376	6.463
Conversion 10 deg	6.404	0.327	6.077
Pin length +10 mm	8.961	0.536	8.425
Pin length – 10 mm	5.695	0.312	5.383
Pin diameter 4 mm	9.670	0.324	9.346
Pin diameter 6 mm	4.941	0.350	4.591
Rotation posterior 10 deg	7.795	0.301	7.493
Rotation anterior 10 deg	6.411	0.323	6.088







4.4 FORCE VS DISPLACEMENT PLOTS JSW

This section explains the effect of each investigated frame adjustment to the total JSW decrease under loading. Therefore force-displacement plots are created for all 4 alterations. Within these plots, the intermittent red line indicates bone contact at 7.2 mm displacement (minimum JSW+ KJD distance). The black intermittent lines resemble different cases of loading.

4.4.1 PIN THICKNESS VARIATIONS

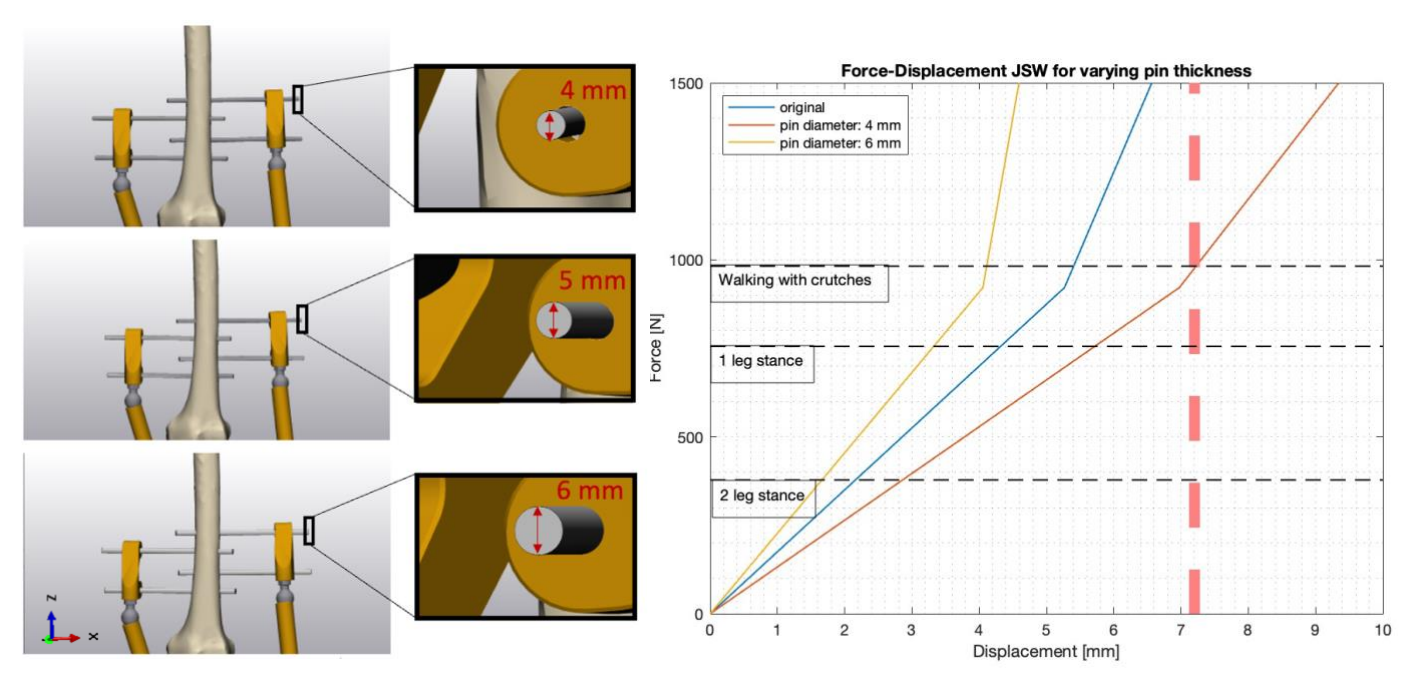


Figure 33 LEFT) Pictures of the adjustments in pin diameter. RIGHT) Decrease of the JSW for three different pin diameters. The intermittent red line resembles the approximate deformation where bone contact could occur.

The stiffness increases when the pin diameter increases. Bone contact at 7.20 mm displacement was observed in the 4 mm diameter pins at 976N of force. Also, an increase in stiffness was visible at the point where the springs were maximally deformed. JSW decrease was $42.3\,\%$ higher and $30.1\,\%$ lower for 4 mm pins and 6 mm pins respectively, as compared to the default pin diameter (5 mm).







4.4.2 PIN LENGTH VARIATIONS

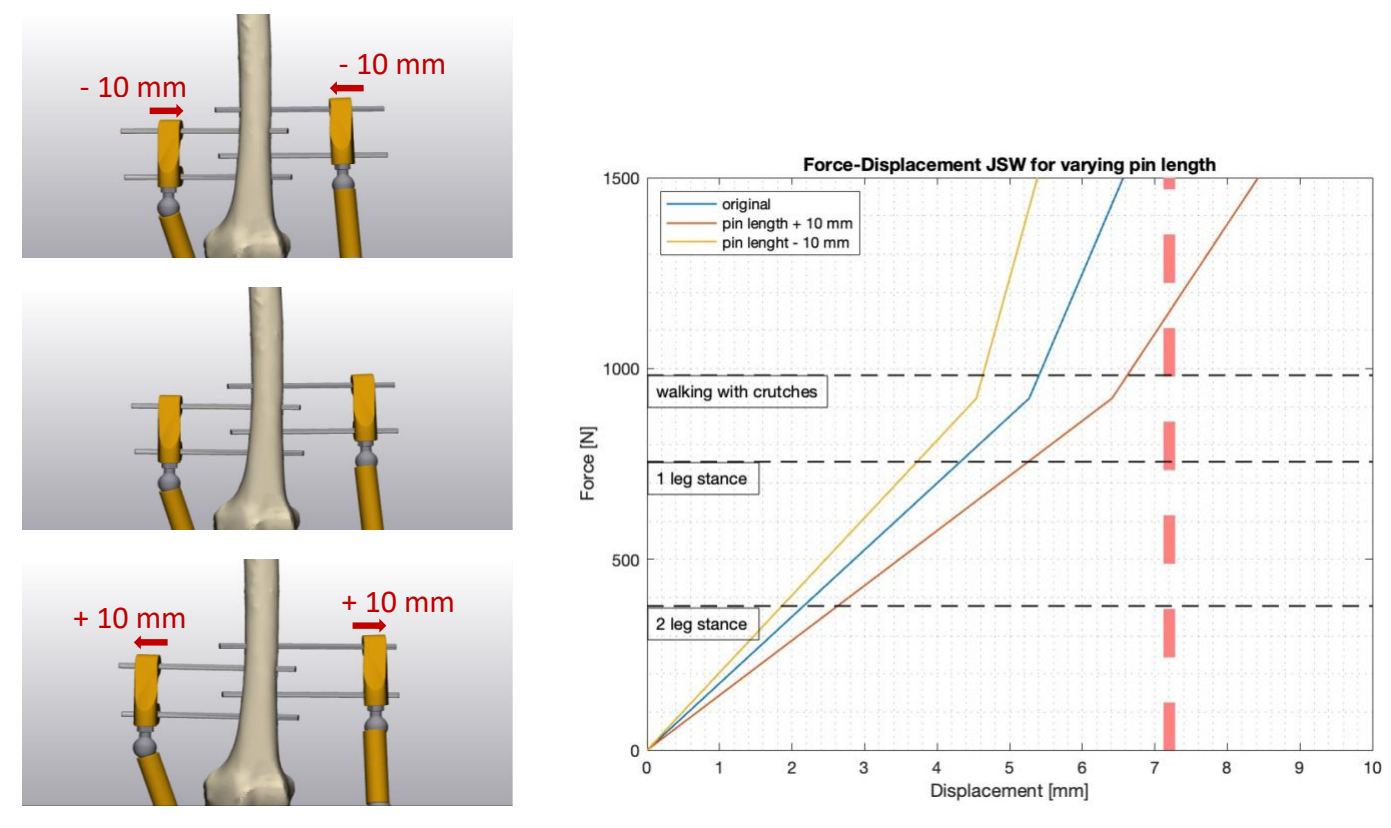


Figure 34 LEFT) Pictures of the adjustments in pin length. RIGHT) Decrease of the JSW for three different pin lengths. The intermittent red line resembles the approximate deformation where bone contact could occur.

The stiffness decreases when the pin length increases. Bone contact at 7.20 mm displacement was observed in the pin length +10 mm situation at a force of 1148 N. Also, an increase in stiffness was visible at the force where the springs were maximally deformed. JSW decrease was 28.3 % higher and 18.1 % lower for 10 mm longer pins and 10 mm shorter pins respectively, as compared to the default pin lengths (Table 1).







4.4.3 INSERTION ANGLE: CONVERGING PINS

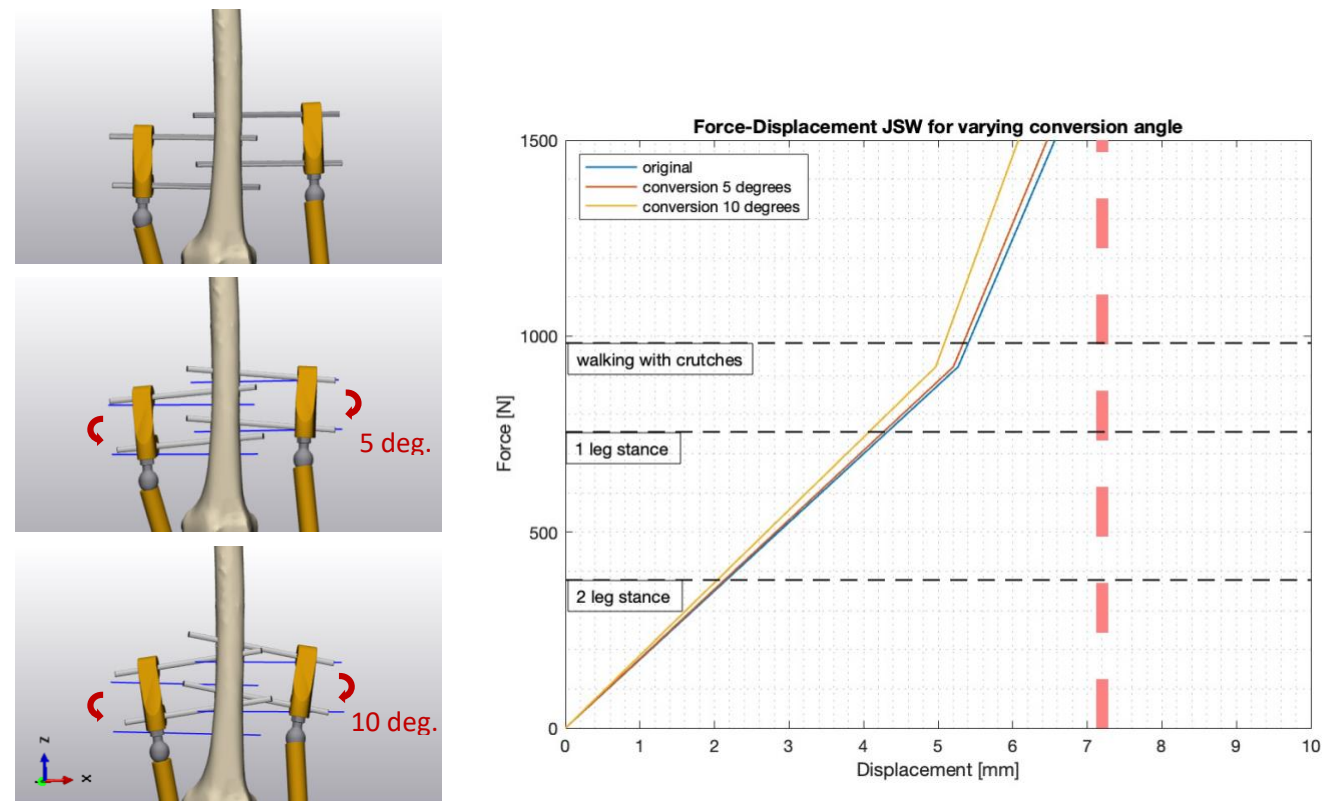


Figure 35 LEFT) Pictures of the adjustments in pin conversion angle. RIGHT) Decrease of the JSW for three different pin angles. The intermittent red line resembles the approximate deformation where bone contact could occur.

The converging pin insertion angles result in a slightly increased frame stiffness. There was no bone contact observed within the range of 1500 N. Again, an increase in stiffness was visible at the force where the springs were maximally deformed. JSW decrease was 1.7 % lower and 7.5 % lower for 5 degrees converted pins and 10 degrees converted pins respectively, as compared to the default pin insertion angles (parallel pins).







4.4.4 INSERTION ANGLE: ROTATED PINS

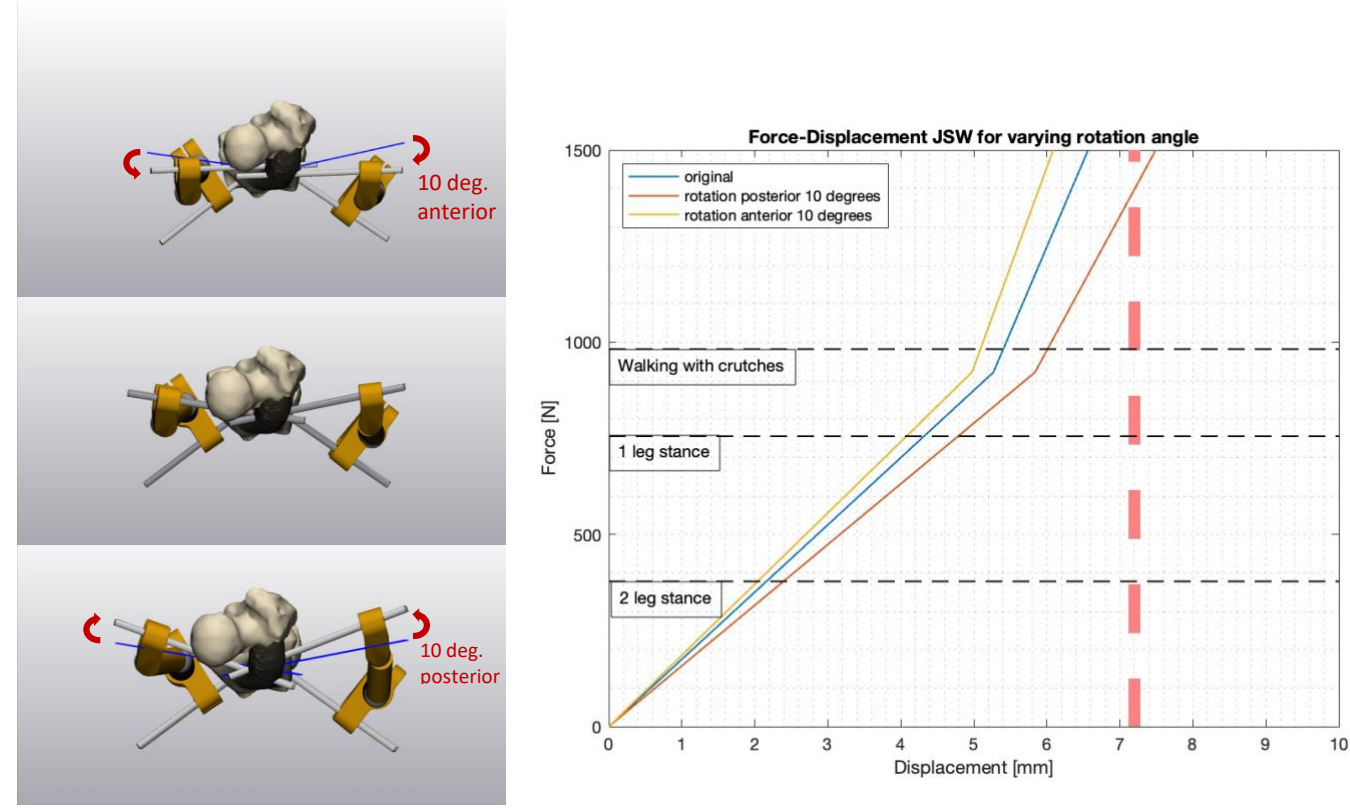


Figure 36 LEFT) Pictures of the adjustments in pin femur rotation angle. RIGHT) Decrease of the JSW for three different pin angles. The intermittent red line resembles the approximate deformation where bone contact could occur.

The anteriorly inserted bone pins resulted in a slightly increased frame stiffness, while posteriorly inserted bone pins resulted in a decreased frame stiffness. Bone contact was observed for the posteriorly inserted pins at a loading force of 1397 N. Again, an increase in stiffness was visible at the force where the springs were maximally deformed. JSW decrease was 14.0 % higher and 7.5 % lower for posteriorly inserted pins and anteriorly inserted pins respectively, as compared to the default pin insertion angles (Figure 6).







4.5 KNEE ROTATIONS

In this section, the relative rotations within the knee joint are displayed (Table 7). Rotations that were mostly observed are: flexion, adduction, and exo-rotation. Table 7 summarizes the different rotations in all tested frame configurations.

Table 7 Relative rotations within the JSW per model adjustment for a vertical load of 1500 $\rm N$

	Angle x deg	Angle y deg	Angle z deg
	(+Extension/ -	(+Adduction/-	(+Exorotation / -
Model	Flexion)	Abduction)	Endorotation)
Original set-up	-1.459	-0.696	0.594
Conversion 5 deg	-1.038	-0.216	0.662
Conversion 10 deg	-1.426	-0.173	0.530
Pin length +10 mm	-0.921	-0.556	0.257
Pin length – 10 mm	-0.937	-3.775	0.322
Pin diameter 4 mm	-1.761	-0.433	0.259
Pin diameter 6 mm	-0.703	-0.321	0.150
Rotation posterior 10 deg	-0.543	-0.186	-0.081
Rotation anterior 10 deg	-2.790	-0.692	0.359







4.6 STRESS CONCENTRATIONS

Figure 37 displays the stresses within the FE model. The stresses in the femoral pins were higher than the stresses in the tibial pins. In the femoral pins, the medial pins showed higher stress concentrations than the lateral pins. For the tibial pins the opposite effect was visible. Maximal principal stress values for each pin are provided in Table 8.

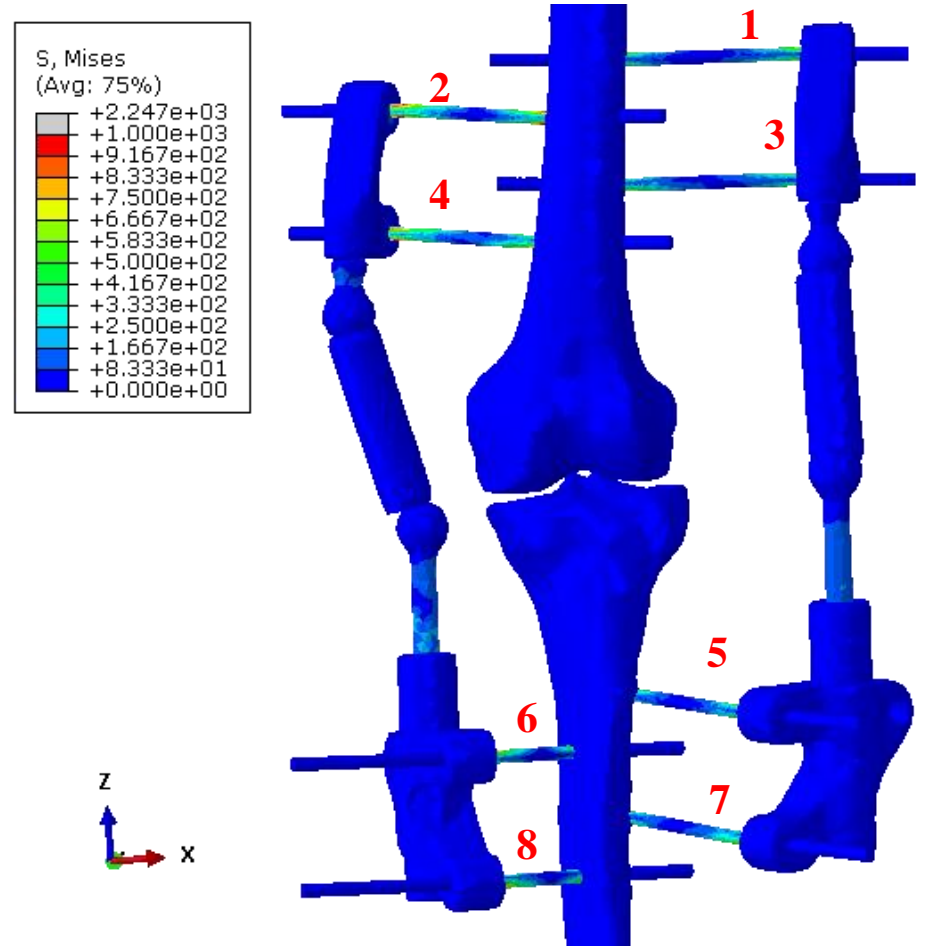


Figure 37 Stress distribution of the pins [MPa] within the original FEM for a vertical (z) loading force of 1500 N. The numbers (1-8) coincide with the pin numbers in Table 8. Highest stress was observed in pin 2.







Table 8 Highest principal stress values [MPa] reported per bone pin under a vertical (z) loading force of 1500 N. Highest pin

principal stress was observed in pin 2.

D	The section of	NA I
Pin nr	Location	Maximal
		principal stress
		[MPa]
1	Lateral femur proximal	1198
	·	
2	Medial femur proximal	2398
	р. с	
3	Lateral femur distal	1396
	Latera Terriar alstar	1330
4	Medial femur distal	2201
4	Mediai femur distai	2301
_		
5	Lateral tibia proximal	1499
6	Medial tibia proximal	1197
7	Lateral tibia distal	1804
8	Medial tibia distal	1103

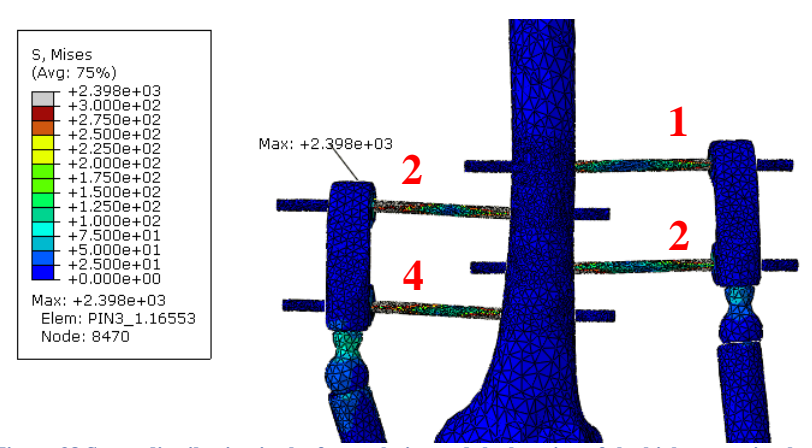


Figure 38 Stress distribution in the femoral pins and the location of the highest maximal principal stress for a vertical loading force of 1500 N. Location of the maximal principal stress value was on the frame side of the pin.

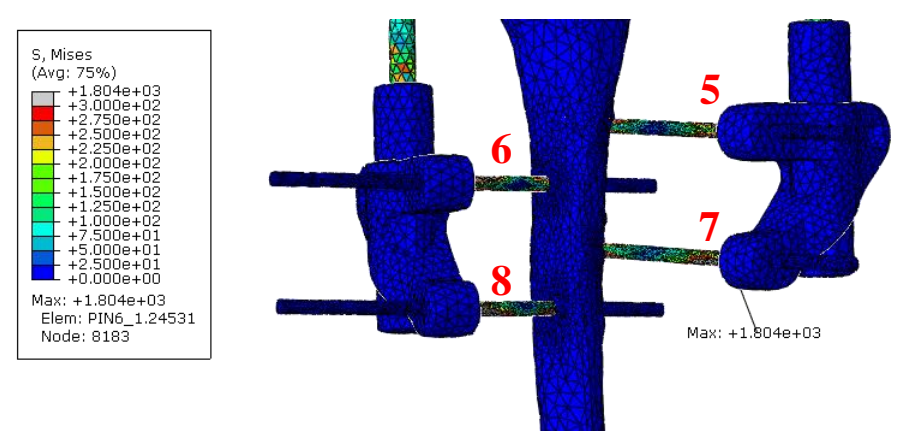


Figure 39 Stress distribution in the tibia pins and the location of the highest maximal principal stress for a loading force of 1500 N. Location of the maximal principal stress value was on the frame side of the pin.







The highest principal stress value in the femoral cortical bone tissue was observed in the distal medial bone pin interaction (229 MPa). For the tibia, the highest principal stress value was also observed in the distal medial bone pin interaction (195 MPa).

4.7 MICROMOTIONS

Micromotions were in the range of 20-100 μm . Largest micromotion was observed in the medial femoral proximal pin (0.095 mm). The smallest micromotion was observed in the medial tibial proximal pin (0.027 mm). Average micromotions for the medial femoral pins are largest and average micromotions for the medial tibial pins are smallest.

Table 9 Pin number, pin location and respective micromotion in um for a vertical load of 1500 N

Pin nr	Location	Micromotion [μm]
1	Lateral femur proximal	63
2	Medial femur proximal	41
3	Lateral femur distal	60
4	Medial femur distal	95
5	Lateral tibia proximal	84
6	Medial tibia proximal	27
7	Lateral tibia distal	35
8	Medial tibia distal	42
1&3	Average lateral femur	68
2&4	Average medial femur	62
5&7	Average lateral tibia	60
6&8	Average medial tibia	35







4.8 RELATIONS FRAME PARAMETERS

In this section, relations are formed between the frame parameters and the JSW decrease. These relations could be used to predict the ideal pin dimensions during KJD treatment. In Figures 40 and 41, the stiffness of the construct is plotted against the pin length and pin diameter. Five blue dots in each plot resemble the results of five FEMs. Three different types of polynomials were fitted to relate the datapoints (blue dots). Mean error values between the datapoints and the polynomials are provided in Tables 10 and 11. Based on these error values, the following relations for pin length and pin diameter were selected:

$$Sl = -0.0831 * L^2 + 3.60 * L + 251$$
 (9)

$$Sd = -9.89 * D^2 + 173 * D - 388 \tag{10}$$

Where:

• **SI** = Stiffness depending on the pin length

• L = Pin length

• **Sd** = Stiffness depending on pin diameter

• **D** = Pin diameter

During optimal KJD treatment, JSW clearance is always maintained. On the other hand, small pin diameters are favored to avoid pin infections and other complications. Therefore, for each patient, the same JSW decrease is desired for an equal loading force, resembling with a constant stiffness. A predictive equation for pin diameter (D) could be formed by compensating the change in stiffness due to pin length changes, with a certain pin diameter. Therefore, Δ SI (stiffness change due to length) should be equal to negative Δ Sd (stiffness change cause by diameter):

$$\Delta Sl = -\Delta Sd \tag{11}$$

Where ΔSI is the difference between the stiffness of the average pin lengths (50 mm) and the stiffness of the patients' pin lengths. ΔSd is the difference between the stiffness of the new pin diameter (D) and the stiffness of the default pin diameter (5 mm). An example of the determination of the ΔSI and ΔSd can be found in Appendix Figures 6 and 7.

$$\Delta Sl = Sl(L) - Sl(50) \tag{12}$$

$$\Delta Sd = Sd(D) - Sd(5) \tag{13}$$

Substituting the previous equations leads to:

$$Sl(L) - Sl(50) = -Sd(D) + Sd(5)$$

Consequently, an expression for D could be formed by substituting Equation 9 and 10, rearranging the terms and applying the quadratic formula:

$$-0.0831 * L^2 + 3.60 * L + 251 - 223 = -(-9.89 * D^2 + 173 * D - 388) + 230$$

$$\mathbf{D} = \frac{173 \pm \sqrt{29929 - 39.56 * (590 + 0.0831 * L^2 - 3.60 * L)}}{19.78} \tag{14}$$







Example using Equation 14:

If the pin lengths would be 10 mm (L=60) longer than the average pin lengths, pin diameters to maintain the stiffness would have to be 5.84 mm. On the other hand, if the pin length would be 10 mm shorter (L=40), pin diameters of 4.51 mm would suffice to maintain the desired stiffness.

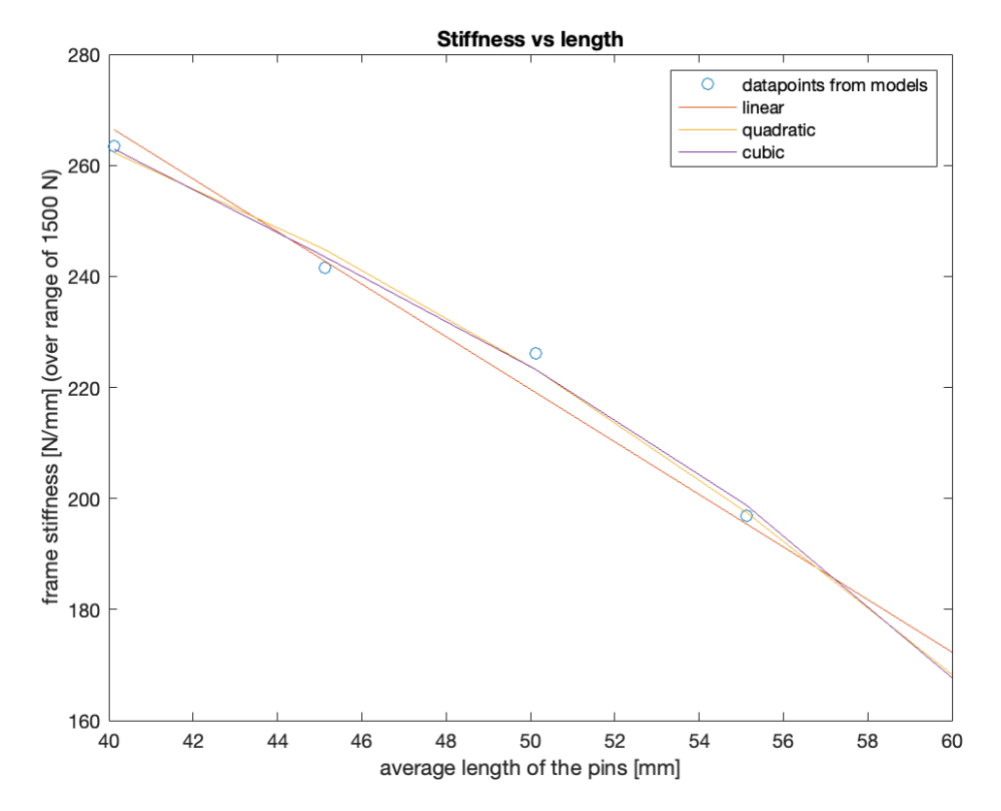
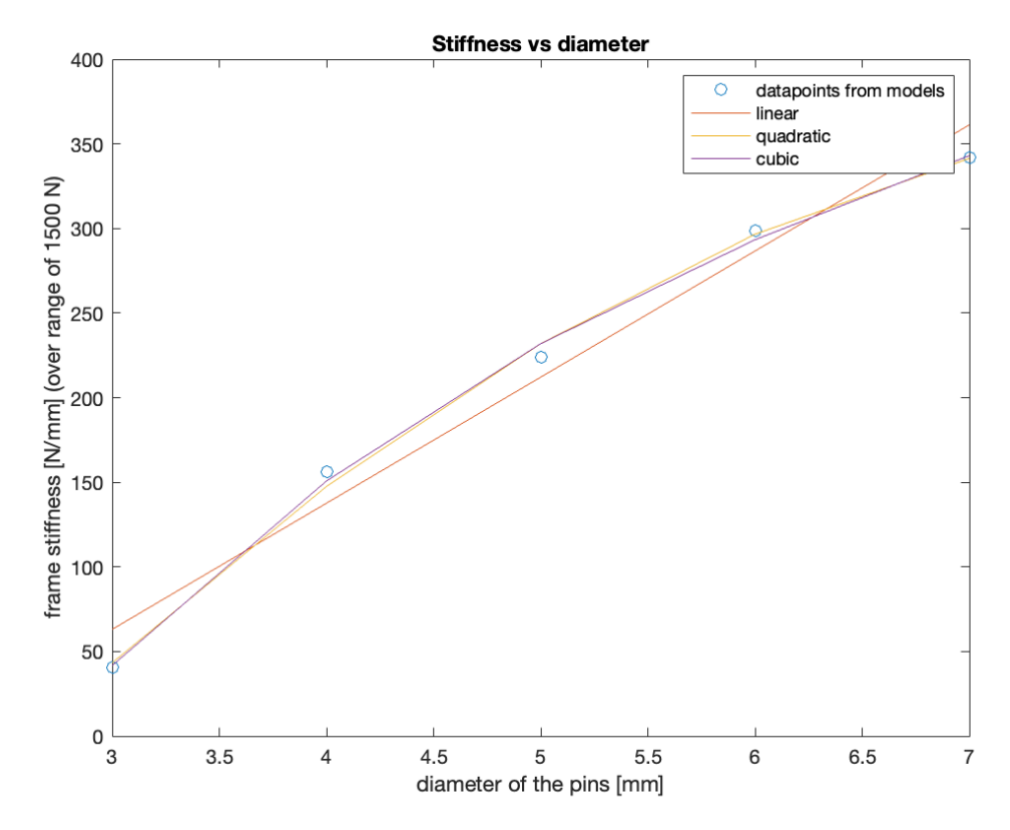


Figure 40 Relations (continuous lines) fitted over the datapoints (blue dots) retrieved from 5 FEMs with modified pin lengths.









Figure~41~Relations~(continuous~lines)~fitted~over~the~datapoints~(blue~dots)~retrieved~from~5~FEMs~with~modified~pin~diameters.

Table 10 Fitted relations between pin length and stiffness including their mean errors. The relation with the smallest error is displayed in hold.

Length			
Туре	Order	Error	Relation
Linear	1	6,12	S _L = -4.73*L + 456
Quadratic	2	3,99	$S_L = -0.0831*L^2 - 3.59*L + 251$
Cubic	3	5,32	$S_L = -0.0043L^3 + 0.569*L^2 - 28.7*L + 779$

Table 11 Fitted relations between pin thickness and stiffness including their mean errors. The relation with the smallest error is displayed in bold.

Diameter			
Туре	Order	Error	Relation
Linear	1	26,6	S _D = 74.5*D - 161
Quadratic	2	10,8	$S_D = -9.89 * D^2 + 173 * D - 388$
Cubic	3	14,6	$S_D = 1.35*D^3 - 30.2*D^2 + 270*D - 534$







5 DISCUSSION

This research used Finite Element Models to investigate the JSW decrease and knee rotations during KJD. A decrease in JSW is observed when the pin thickness decreased, and pin length increased. Quadratic polynomials appeared to describe the relation between pin diameter and frame stiffness most accurately. Also, the relation between pin thickness and frame stiffness is most accurately described by a quadratic polynomial.

For different insertion angles, a smaller clinically irrelevant effect was found. The stiffness increased slightly when the pins were converged in the coronal plane. Moreover, stiffness increased while the femoral pins were placed anterior and decreased while the pins were placed posterior. Relative knee rotations were mainly in flexion, abduction, and exo-rotation direction, and their magnitude depended on the frame alterations. Within the original set-up (pin length derived from Table 1, pin diameter 5mm), micromotions between the frame and the pins were biggest for the most distal medial femoral pin. Also, the highest stress concentrations were found within the medial femoral pins.

5.1 LIMITATIONS

Non-linear elastic deformation is often observed in the deformation of objects in the real-world. However, due to their computational efficiency, linear models were used in the current project. An efficient computational time is convenient to investigate many frame parameters. Furthermore, linear models are accurate for small strains. Considering the displacement is several millimetres, linear models are chosen in the current research.

Ligaments, tendons, or muscles surrounding the knee joint can cause a pre-tension effect which could affect the distraction distance. The effect that pre-tension could have on the distraction distance is not included in the model because its magnitude is unknown. The JSW is thus increased by 5 mm in the FEM, while in-vivo the distraction distance could be smaller.

There are two options to model a connection between two parts in finite element analysis software. One option is to use a tie. This is computationally the most efficient option because it fixes the position of both parts relative to each other. The tie function introduces compressive and tensile stresses to the material that is assigned for the connection. Another option is to use an interaction to connect both surfaces. With the interaction function, only compressive forces will be exerted. In distraction treatment, it is questionable which method is most accurate. On one hand, osseointegration could occur resulting in pins that are fixed using both compressive and tensile forces. On the other hand, considering the average distraction treatment of 6 weeks, osseointegration is often in the beginning stages (Gathen et al., 2019). Furthermore, the pins used by ArthroSave do not have a coating to facilitate osseointegration. Therefore, it can be assumed that only compressive forces are transferred at the bone pin interaction. In KJD treatment, the connection between bone and bone pin could also be a combination of a tie and an interaction.

The ArthroSave 'KneeReviver' intends to allow intermittent fluid pressure in the JSW during loading. This effect is accounted from by springs that decrease the stiffness of the frame. During the







experimental tests performed by BAAT medical, there was no stiffness change observed around 921.6 N. This suggests that the springs were not compressed maximally during these tests. A reason for this could be the malfunctioning of the springs in the experimental set-up. Considering the original design of the springs, these experimental tests are not replicated but the intended spring behaviour is included in the FEM.

The validation procedure was performed using a PE validation FEM. From this validation could be concluded that the mechanical behaviour of the FEM resembled the behaviour of the experimental test. The method for building the FEM was thus accurate. A next step would be to ensure that the deformation of the bone FEM also corresponds with the deformation in a real patients knee joint. It is expected that soft tissues will significantly influence the deformation. The knee joint model could be validated ex-vivo by applying the KJD frame to a cadaver specimen under an applied load and measure the JSW. Also, a new patient trial is planned in UMC Utrecht where knee OA patients will receive KJD treatment. During this trial, strain gauges could be applied to the frame to establish the force transmitted by the frame in vivo. Unfortunately, the trial could not be combined with the current research. Nevertheless, based on the validation model and the repeatability of FEM, there is confidence in the accuracy of the current FEMs.

The load applied to the model in this research was a rough estimate of what the loading could be during KJD treatment. It is not yet quantified in vivo how much force will be exerted on the frame while walking or standing.

In this project, three different loading cases were visualized. These loading cases are arbitrary and influenced by the patient's loading behaviour. In this research, results are computed for vertical forces up to 1500 N. In reality, the loading forces could even exceed this value, depending on the loading behaviour. Furthermore, the direction of the load was not altered within this research. During walking, forces are presumably exerted on the leg in multiple directions. Again, due to a lack of quantification of the in-vivo loading forces, the direction of the force was unknown. A vertical loading force was therefore assumed.

5.2 INTERPRETATION

The results of the JSW decrease based on parameters changes (pin length, pin diameter and pin insertion angles) largely matched the expected outcomes. Based on knowledge on pin deformation (Timosjenko, 1953), the JSW decrease was expected to be larger with longer pins and smaller with shorter pins. Also pins with smaller diameters were expected to result in more JSW decrease and the other way around. The relation between pin thickness and length was quadratic. Yet, following equation 3, the pin bending depends on pin thickness to the power 4 and pin length to the power 3. Nonetheless, the quadratic relation is plausible because the JSW decrease is not solely depending on pin deformation but there is also spring deformation and potentially some deformation in different parts of the frame. Pin insertion angles changes around the y-axis were expected to result in a stiffer system, however the results showed a very small stiffness increase. The stiffness changes due to pins rotated around the z-axis was considerable.

The JSW decrease of the original frame FEM (~6.5 mm) can be compared with the theoretic JSW decrease calculation (~8.35 mm). This difference (~1.85 mm) could be explained by some factors. Firstly, the theoretical calculations are based on a 2D free body diagram. This means that insertion angles and bone geometries are not included. Therefore, all forces are only working in the vertical direction. Contrarily, due to the 3D geometry in the FEM, forces could cause bending moments (knee







flexion as observed in Figure 24, upper left picture) that will not result in JSW decrease. Furthermore, the pin deflecting for a single pin (Equation 3) was a simplification of the theoretic pin deflection that would be the most accurate. In Appendix Figure 5, this effect is elaborated. Another factor could be that the length of the pins was assumed to be equal for all pins, while in the model the pin lengths were varying. Furthermore, the interaction between the bone and pins was fully fixated in the analytical calculations while only compressive forces were transferred in the FEMs. Regarding FEM experiment displayed in Appendix Figure 1, this fixation could account for a stiffness difference of ~16 percent. Lastly, the forces were assumed to be equally distributed amongst all pins. This did not occur in the FEM and is also unlikely to happen in in-vivo KJD treatment of patients. Altogether, the difference observed emphasises the use of FEMs in biomechanical orthopaedic research.

The relations retrieved in Section Relations Frame Parameters can be useful in clinical settings because they could function as a guideline for the bone pin selection. First, a clinician would determine the potential pin length of a patient. Then, based on this pin length, the clinician could pick a pin that is suitable for this patient such that there is no bone-on-bone contact in any loading situation and the pin thickness is also minimized to reduce the risk on pin tract infections. This could lead to more efficient treatment and potentially better clinical outcomes for the patients. The relation between pin length and thickness that results from this research is a step in a bigger process of creating patient specific KJD treatment. The fitting parameters in the relation should be subjected to more extensive further research.

Observations from UMC Utrecht reported high infection rates for the medial femur pins. The highest stress concentrations are also observed in these pins. Although relatively small (<100 μ m) compared to micromotions reported in systematic research papers (20 – 800 μ m, Kohli et al, 2021), the largest micromotions also occurred in the medial femoral pins.

As mentioned before, pin lengths are largely depending on the surrounding soft tissue size. In most cases, the femur has more surrounding soft tissue than the tibia. Also, the size of the soft tissue on the medial side of the tibia is considerably smaller than on the lateral side. This results in in unequal pin lengths (Table 1). While in-vivo loading, the knee joint is stabilized by ligaments and tendons. Therefore, the deformation will dominantly happen in the vertical direction. Thus, the medial femoral pins will presumably take up more of the force and will deform more. Pin tract infection could be induced by these micromotions and stress concentrations. The presence of pin tract infections will result in complication in the KJD treatment and potentially less beneficial clinical results.

Maximal stresses in some locations were high. The maximal stresses on the cortical bone (max 229 MPa in the femur, max 195 MPa in the tibia) were close but not exceeding the yield stress of cortical bone (Toma et al, 1997). Stresses on the pins (Table 8) did exceed the yield stress for stainless steel (~300 MPa) (Tylek and Kuchta, 2014). Therefore, there could be a chance plastic deformation and/or fatigue in the pins. An important note is that these stress values were computed for a load of 1500 N, while it is unknown if this load is applied in-vivo. Stress values for FEMs must be carefully interpreted. To accurately examine stress distributions, further mesh convergence investigating max stress values is required. The mesh convergence in this research was mainly performed to investigate the displacement of the pins. Furthermore, the connection between the bone pins and the blocks of the frame (completely fixed) could cause inaccurately high stresses in the pins.







5.3 CONCLUSIONS

Based on this research the following conclusions can be made:

- Although patients have varying knee anatomy loading behaviour, the distraction of 5 mm might be undone during loading in KJD treatment. Also, bone-on-bone contact between surfaces of the femur and tibia could occur within the force range that is applied during normal walking without crutches. While walking with crutches, the risk of bone-on-bone contact is minimal.
- Alterations to the existing ArthroSave KJD frame during loading resulted in:
 - o Thicker and shorter pins resulted in less JSW decrease.
 - o Thinner and longer pins resulted in more JSW decrease.
 - Pins that were inserted with a converging angle resulted in slightly less JSW decrease. However, the size of this effect seems clinically irrelevant.
 - Pins that were inserted with an anterior rotation around the longitudinal axis resulted in more JSW decrease. Controversially, pins that were inserted with a posterior rotation resulted in more JSW decrease.
- Relative knee rotations occurred mostly in the flexion, abduction and exo-rotation directions. These rotations were dependent on different frame alterations.
- Micromotions between the pin and bone and stress concentrations in the pins are
 predominantly observed in the medial femoral pins and could be explained by differences
 between pin lengths.
- Based on this research Finite Element Models, a quadratic relation between pin length and pin diameter of the KJD device could be derived. This relation could provide as a guideline for the selection of patient-specific pins, which could be a step in a bigger process of realizing patient-specific KJD treatment.

5.4 COMPARISON OTHER PAPERS

As far as known, no research has been performed building FEMs of KJD. However, FEM research was performed on ankle joint distraction. Nielsen et al. (2005) published a paper that focusses on determination of the ankle external fixation stiffness using an Illizarov ring frame. They modified various parameters of the frame, including the pin diameters. They observed a reduced tibia displacement of 20.6 % for 7 mm pins with respect to 6 mm pins. While reducing the pin diameter to 5 and 4 mm, an increased displacement of 37.8 % and 84.4 % respectively was found. They also observed that placing the tibia closer to the ring of the fixator, would increase the system stiffness. Although varying displacement numbers, these findings coincide with the results of this research.

Pervan and colleagues (2022) analysed the biomechanical performance of a monolateral external fixator device. They investigated pin insertions angles of the frame and found that a construction with parallel pin placement had lower displacement values than a construction with pins placed in a respective angle for stainless steel frames. Interestingly, for carbon frames, the opposite effect was found. This emphasises the relevance of frame material properties in such calculations. They also investigated stresses in critical zones and found about 33 % less stress in critical zones for carbon frames. These frames would thus, benefit the bone pin interactions by introducing lower peak stresses leading to less chance of pin failure.







5.5 FURTHER RESEARCH

High numbers of pin tract infections are complicating KJD treatment. Further research could therefore examine the impact of varying individual pin lengths on bone versus pin micromotion and the occurrence of pin tract infections. Within the available UMC Utrecht database, the relation between pin length and pin tract infection of a specific pin could be investigated. This way it could become clear whether pin lengths influence pin infections in-vivo. Furthermore, FEM could be used to examen frame set-ups where individual pin lengths are modified. The JSW decrease, rotations, micromotions and stress concentrations could be compared for different pins.

The current research FEMs were a simplification of the in-vivo mechanical behaviour of the ArthroSave KJD frame. Bone geometries and bone materials have been included in the current FEMs. In further FEM research of this frame, an even more realistic model could be created. Soft tissues like articular cartilage with non-linear material properties could be included. Unfortunately, only having access to CT images, the geometry of the articular cartilage was not available. Magnetic Resonance Imaging (MRI) data is required to extract soft tissue geometries. Other important soft tissue structures would be the ligaments, tendons and muscles that surround the knee joint. These structures are expected to stabilize the knee joint. For this stabilization, they exert forces passively and/or actively. Considering these structures can only generate pulling forces and no pushing forces, forces within the knee joint might be higher with these structures included. Also, because of the stabilizing effect, the rotations observed in the FEMs could be less than the rotations observed in this research. Moreover, it is important to perform extensive validation while creating FEMs that include cartilage, ligaments, tendons and/or muscles.

To generate more confidence in the relation between pin length and pin thickness, more FEMs could be used. Now, 5 FEMs have been created to generate 5 datapoints for each parameter (Figures 40 and 41). The amount of FEMs could be extended to retrieve a higher number of datapoints. Also, the bodyweight of a patient, which is relatively easy to measure, could be included in this relation. Bodyweight has an expected large impact on the load applied to the treated knee and is not included in the current research. Within the prediction of pin thickness, patients' bodyweight could be a variable factor.

Further research might also be performed on the functioning of the springs integrated in the monotubes of the ArthroSave frame. During the BAAT medical experimental tests, the functioning of the springs was not evident. To establish the actual mechanical behaviour of the frame, it is important to check the functioning of these springs.

Lastly, to determine accurate loading forces, in-vivo clinical measurements on walking behaviour are required. These measurements could be performed in prospective clinical patient trials in UMC Utrecht.







6 BIBLIOGRAPHY

- Albrektsson, T., & Johansson, C. (2001). Osteoinduction, osteoconduction and osseointegration. *European spine journal*, 10(Suppl 2), S96-S101.
- Aro, H. T., Markel, M. D., & Chao, E. Y. (1993). Cortical bone reactions at the interface of external fixation half-pins under different loading conditions. *Journal of Trauma and Acute Care Surgery*, 35(5), 776–785.
- Baskin, M. L., Ard, J., Franklin, F., &, & Allison, D. B. (2005). Prevalence of obesity in the United States. *Obesity Reviews*, 6(1), 5–7.
- Bayliss, L. E., Culliford, D., Monk, A. P., Glyn-Jones, S., Prieto-Alhambra, D., Judge, A., ... &, & Price, A. J. (2017). The effect of patient age at intervention on risk of implant revision after total replacement of the hip or knee: a population-based cohort study. *The Lancet*, 389(10077), 1424–1430.
- D'Ambrosia, R. D. (2005). Epidemiology of osteoarthritis. Orthopedics, 28(2), S201-S205.
- Drijber, F. P., Finlay, J. B., & Dempsey, A. J. (1992). Evaluation of linear finite-element analysis models' assumptions for external fixation devices. *Journal of biomechanics*, 25(8), 849-855.
- Frost, H. M. (1994). Frost, H. M. (1994). Wolff's Law and bone's structural adaptations to mechanical usage: an overview for clinicians. *The Angle Orthodontist*, 64(3), 175–188.
- Gathen, M., Ploeger, M. M., Jaenisch, M., Koob, S., Cucchi, D., Kasapovic, A., ... & Placzek, R. (2019). Outcome evaluation of new calcium titanate schanz-screws for external fixators. First clinical results and cadaver studies. Journal of Materials Science: Materials in Medicine, 30, 1-8.
- Haut Donahue, T. L., H. M. L., R. M. M., & J. C. R. (2002). A finite element model of the human knee joint for the study of tibio-femoral contact. *Journal of Biomechanical Engineering*, 124(3), 273–280.
- Hölzer, A., Schröder, C., Woiczinski, M., Sadoghi, P., Scharpf, A., Heimkes, B., & Jansson, V. (2013). Subject-specific finite element simulation of the human femur considering inhomogeneous material properties: A straightforward method and convergence study. *Computer Methods and Programs in Biomedicine*, 110(1), 82–88. https://doi.org/10.1016/j.cmpb.2012.09.010
- Intema, F., Wiegant, K., van Roermund, P. M., Marijnissen, A. C., Cotofona, S., Felix, E., ... &, & Lafeber, F. P. (2010). Tissue Structure modification in end stage knee osteoarthritis by use of joint distraction. . *Osteoarthritis Cartilage*, 18(2), S142.
- Jansen, M. P., Boymans, T. A. E. J., Custers, R. J. H., van Geenen, R. C. I., van Heerwaarden, R. J., Huizinga, M. R., Nellensteijn, J. M., Sollie, R., Spruijt, S., & Mastbergen, S. C. (2021). Knee Joint Distraction as Treatment for Osteoarthritis Results in Clinical and Structural Benefit: A Systematic Review and Meta-Analysis of the Limited Number of Studies and Patients Available. In *Cartilage* (Vol. 13, Issue 1_suppl, pp. 1113S-1123S). SAGE Publications Inc. https://doi.org/10.1177/1947603520942945
- Jansen, M. P., Mastbergen, S. C., van Heerwaarden, R. J., Spruijt, S., van Empelen, M. D., Kester, E. C., Lafeber, F. P. J. G., & Custers, R. J. H. (2020). Knee joint distraction in regular care for treatment of knee osteoarthritis: A comparison with clinical trial data. *PLoS ONE*, 15(1). https://doi.org/10.1371/journal.pone.0227975
- Jansen, M. P., van Egmond, N., Kester, E. C., Mastbergen, S. C., Lafeber, F. P. J. G., & Custers, R. J. H. (2020). Reduction of pin tract infections during external fixation using cadexomer iodine. *Journal of Experimental Orthopaedics*, 7(1). https://doi.org/10.1186/s40634-020-00305-y
- Kardux, F. (2020). Finite Element Analysis of external fixation frame with intended use for knee joint distraction. *UMC Utrecht Internal Research*.
- Kellgren, J. H., & Lawrence, J. S. (1957). radiological assessment of osteoarthritis. Ann. Rheum. Dis, 494-501.
- Knecht, S., Vanwanseele, B., & Stüssi, E. (2006). A review on the mechanical quality of articular cartilage Implications for the diagnosis of osteoarthritis. In *Clinical Biomechanics* (Vol. 21, Issue 10, pp. 999–1012). https://doi.org/10.1016/j.clinbiomech.2006.07.001
- Kohli, N., Stoddart, J. C., & van Arkel, R. J. (2021). The limit of tolerable micromotion for implant osseointegration: a systematic review. *Scientific Reports*, 11(1), 1-11.
- Kutzner, I., Heinlein, B., Graichen, F., Bender, A., Rohlmann, A., Halder, A., Beier, A., & Bergmann, G. (2010). Loading of the knee joint during activities of daily living measured in vivo in five subjects. *Journal of Biomechanics*, 43(11), 2164–2173.
- Lee, R., & Kean, W. F. (2012). Obesity and knee osteoarthritis. Inflammopharmacology, 20, 53-58.
- Lenarz, C., Bledsoe, G., & Watson, J. T. (2008). Circular external fixation frames with divergent half pins: A pilot biomechanical study. *Clinical Orthopaedics and Related Research*, 466(12), 2933–2939. https://doi.org/10.1007/s11999-008-0492-0
- Mahir, L., Belhaj, K., Zahi, S., Azanmasso, H., Lmidmani, F., & el Fatimi, A. (2016). Impact of knee osteoarthritis on the quality of life. *Annals of Physical and Rehabilitation Medicine*, 155–159.
- Nielsen, J. K., Saltzman, C. L., & Brown, T. D. (2005). Determination of ankle external fixation stiffness by expedited interactive finite element analysis. *Journal of orthopaedic research*, 23(6), 1321-1328.
- Pervan, N., Mešić, E., Muminović, A. J., Delić, M., Muratović, E., Trobradović, M., & Hadžiabdić, V. (2022).

 Biomechanical Performance Analysis of the Monolateral External Fixation Devices with Steel and Composite Material Frames under the Impact of Axial Load. *Applied Sciences*, 12(2), 722.
- Roermund, P.M., (unknown). Surgical technique 'ArthroSave's KneeReviver'. ArthroSave internal document







- Seitz Jr, W. H., Froimson, A. I., Brooks, D. B., Postak, P. D., Parker, R. D., LaPorte, J. M., & Greenwald, A. S. (1990). Biomechanical Analysis of Pin Placement and Pin Size for External Fixation of Distal Radius Fractures. *Clinical Orthopaedics and Related Research* (1976-2007), 251, 207-212.
- Shelburne, K. B., Torry, M. R., & Pandy, M. G. (2005). Muscle, ligament, and joint-contact forces at the knee during walking. *Medicine and Science in Sports and Exercise*, *37*(11), 1948–1956. https://doi.org/10.1249/01.mss.0000180404.86078.ff
- Smits, J., Cloostermans, V., (2016), Mechanical validation ArthroSave knee reviver
- Stallard, J., Dounis, E., Major, R. E., & Rose, G. K. (1980). One leg swing through gait using two crutches: An analysis of the ground reaction forces and gait phases. *Acta Orthopaedica*, 51(1–6), 71–77. https://doi.org/10.3109/17453678008990771
- Terzini, M., Sicuranza, S., Alberghina, F., Ravera, L., Aloj, D. C., & Bignardi, C. (2021). Evaluation of the Structural Behaviour of a Unilateral External Fixator for Osteosynthesis. *The Open Biomedical Engineering Journal*, 15(1), 29–36. https://doi.org/10.2174/1874120702115010029
- Timosjenko, S. (1953). History of strength of materials McGraw-Hill in New York. McGraw-Hill .
- Toma, C. D., Ashkar, S., Gray, M. L., Schaffer, J. L., & Gerstenfeld, L. C. (1997). Signal transduction of mechanical stimuli is dependent on microfilament integrity: identification of osteopontin as a mechanically induced gene in osteoblasts. *Journal of Bone and Mineral Research*, 12(10), 1626-1636.
- Tylek, I., Kuchta, K. (2014). Mechanical properties of structural stainless steels. *Technical transitions civil engineering*. van der Woude, J. T. A. D., Wiegant, K., van Roermund, P. M., Intema, F., Custers, R. J. H., Eckstein, F., van Laar, J. M., Mastbergen, S. C., & Lafeber, F. P. J. G. (2017). Five-Year Follow-up of Knee Joint Distraction: Clinical Benefit and Cartilaginous Tissue Repair in an Open Uncontrolled Prospective Study. *Cartilage*, 8(3), 263–271. https://doi.org/10.1177/1947603516665442
- van Valburg, A. A., V. R., H. L., L. F. P., & Bijlsma, J. W. (1998). Beneficial effects of intermittent fluid pressure of low physiological magnitude on cartilage and inflammation in osteoarthritis. An in vitro study. . *The Journal of Rheumatology*, 25(3), 515–520.
- Taylor, S. J. G., & Walker, P. S. (2001). Forces and moments telemetered from two distal femoral replacements during various activities. *Journal of biomechanics*, 34(7), 839-848.
- Weber, M., Renkawitz, T., Voellner, F., Craiovan, B., Greimel, F., Worlicek, M., Grifka, J., & Benditz, A. (2018). Revision Surgery in Total Joint Replacement Is Cost-Intensive. *BioMed Research International*, 2018.
- Wheeler, J. L., Cross, A. R., & Rapoff, A. J. (2002). A comparison of the accuracy and safety of vertebral body pin placement using a fluoroscopically guided versus an open surgical approach: an in vitro study. *Veterinary Surgery*, 31(5), 468-474.
- World Health Organization. (2022). WHO European regional obesity report 2022. World Health Organization. Regional Office for Europe.







7 APPENDIX

7.1 MODEL CREATION STEPS

The 3D finite element model of the distraction frame and femoral and tibial bones was created within 33 steps as listed below:

- 1. Importing the DICOM file into Mimics
- 2. Thresholding for Bone density. This was performed by using the Hounsfield units that resemble bone (HU 226-1686). Therefore, all bone material was highlighted in the slices.
- 3. Removing all slices above femur and below tibia.
- 4. Removing the kneecap slice-by-slice using the multiple slice edit tool.
- 5. Separating the femur and tibia by using the split mask tool
- 6. Generate the 3D part in Materialise Mimics.
- 7. Export generated 3D model to Materialize 3-Matic.

In 3-Matic software (Materialise, BE) the following steps were performed:

- 8. Post processing of 3D bone models.
- 9. Creating 8 pins: Cylinders in Materialized 3-Matic
- 10. Positioning pins to the right location according to Figure 6. This process is performed by hand using guidelines in 3-Matic.
- 11. Import CAD files from the ArthroSave frame (provided by ArthroSave BV)
- 12. Orientate frame parts such that they are lined up with the pins, and the pin lengths are matching the average pin lengths as described in Table 1 in Background.

Next steps (13-19) are performed by python script in Materialise 3-Matic:

- 13. Distracting femur part 5 mm in longitudinal direction
- 14. Creating pins with adjustable radius in the same orientation as the pins in step 12.
- 15. Changing pin length with respect to the length described in step 12.
- 16. Entering an adjusted insertion angle for the pins.
- 17. Semi-automatic positioning of the connection part of the frame.
- 18. Creating holes in the bones by using the Subtracting tool to subtract the pin volumes from the tibia and femur.
- 19. Creating volumetric mesh with adaptive mesh size depending on the position of the pins
- 20. Undo femur distraction such that the original position is maintained and corresponds with the segmented position.
- 21. Exporting to Materialise Mimics

Again, in Materialise Mimics the next steps are carried out:

- 22. Assign material properties based on Hounsfield units in Materialise Mimics.
- 23. Export the volume mesh including material properties as an Abaqus .inp file.

In Abaqus CAE the next steps are carried out:

- 24. Frame parts and pin materials are assigned
- 25. Frame parts are connected using Tie constraints.
- 26. Pins are connected to blocks of the frame parts

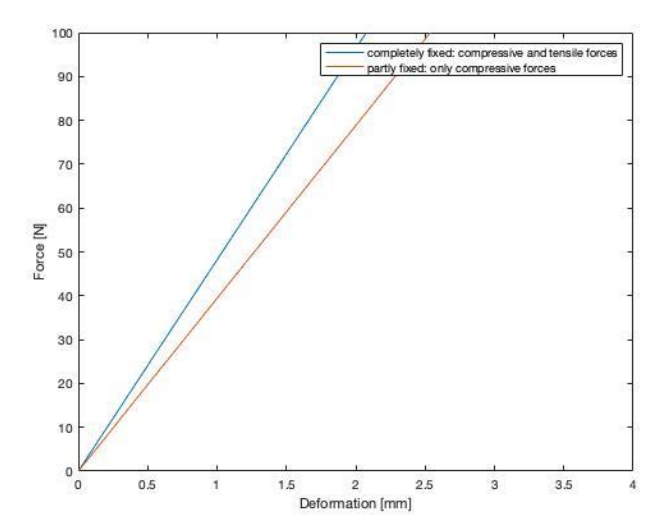






- 27. Pins are connected to bones using the Tie/Interaction function. See Chapter ... for further details about the connection of pins and bones.
- 28. Boundary conditions are set. See Section Boundary Conditions for further details.
- 29. Loading conditions are set. See Section Loading Conditions for further details.
- 30. Run finite element model in Abaqus.
- 31. Examine stresses and strains in Abaqus CAE viewport.
- 32. Retrieve Force-Deformation data.
- 33. Plot stiffness graphs.

7.2 ADDITIONAL FIGURES



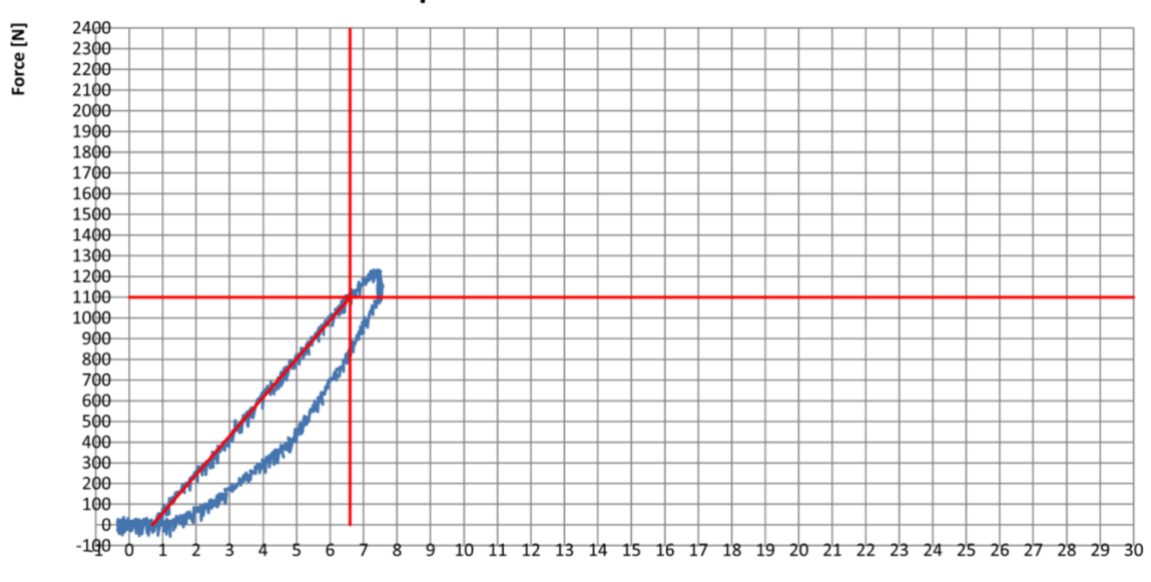
Appendix Figure 1 Stiffness difference for completely fixated pins (tensile forces and compressive forces) and partly fixated pins (compressive forces only)







Static compression



Sample: 1
Appendix Figure 2 Force-Displacement graph of the first BAAT experimental axial loading test

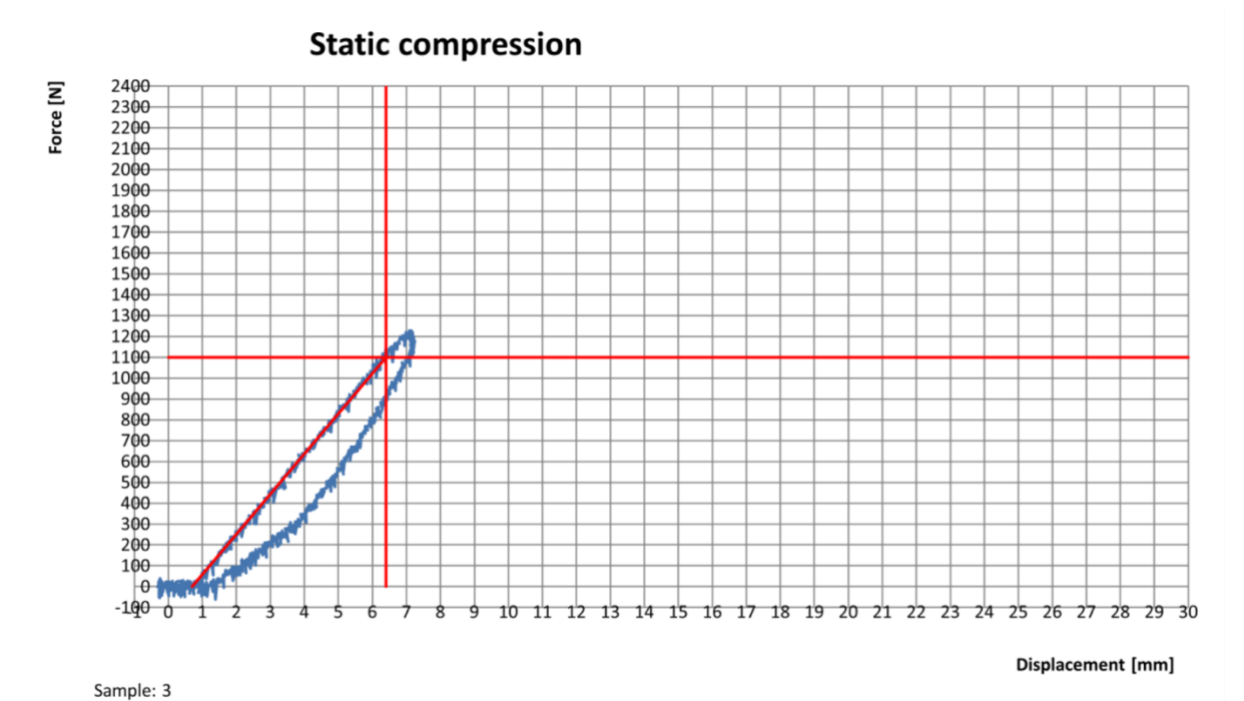
Sample: 2 Appendix Figure 3 Force-Displacement graph of the second BAAT experimental axial loading test



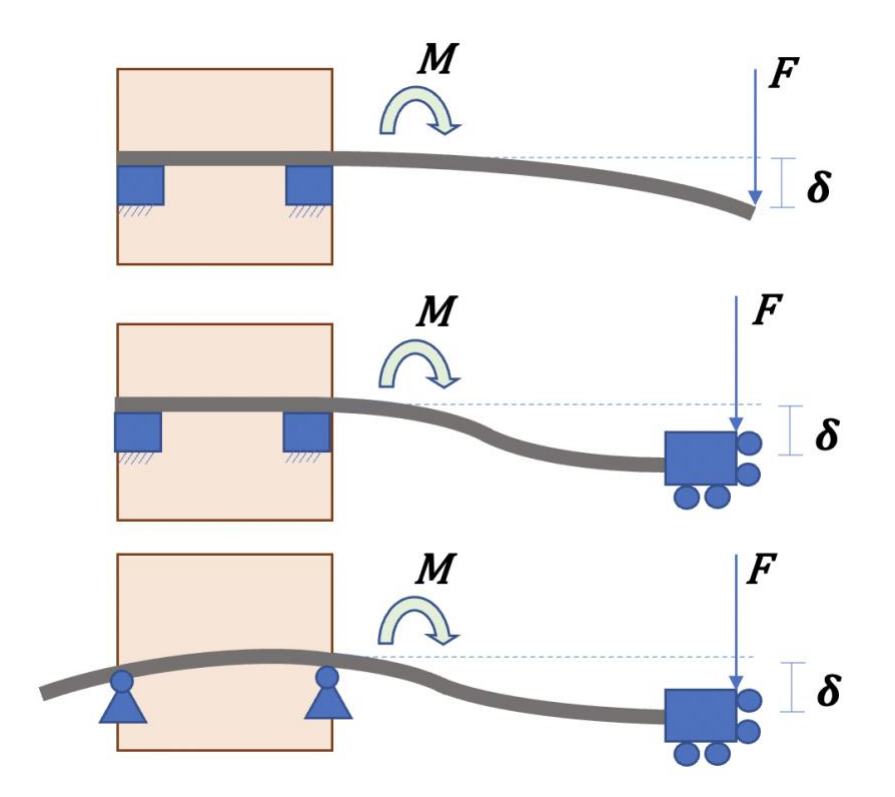




Displacement [mm]



Appendix Figure 4 Force-Displacement graph of the third BAAT experimental axial loading test

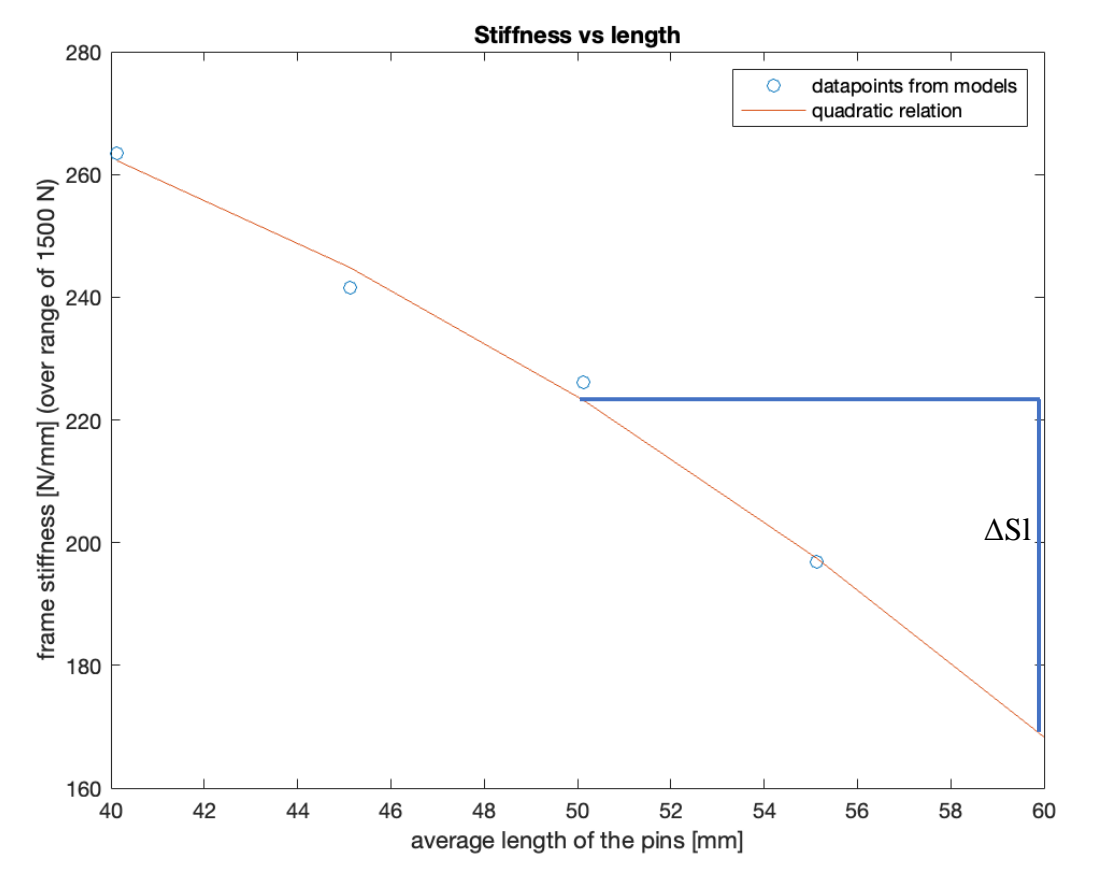


Appendix Figure 5 Potential ways of pin deformation. Upper picture shows a fixed pin that is free to move on the right end. Middle picture shows a fixed pin that has a rolling constraint at the end such that it can only move in horizontal and vertical direction, but it cannot rotate (angle = 0). Lower picture shows a pin that free to rotate, but the deformation is constraint at two points (cortical bone connections). Also, the end of the pin is not allowed to rotate. The bottom picture most accurately resembles with the pins in the FEMs.

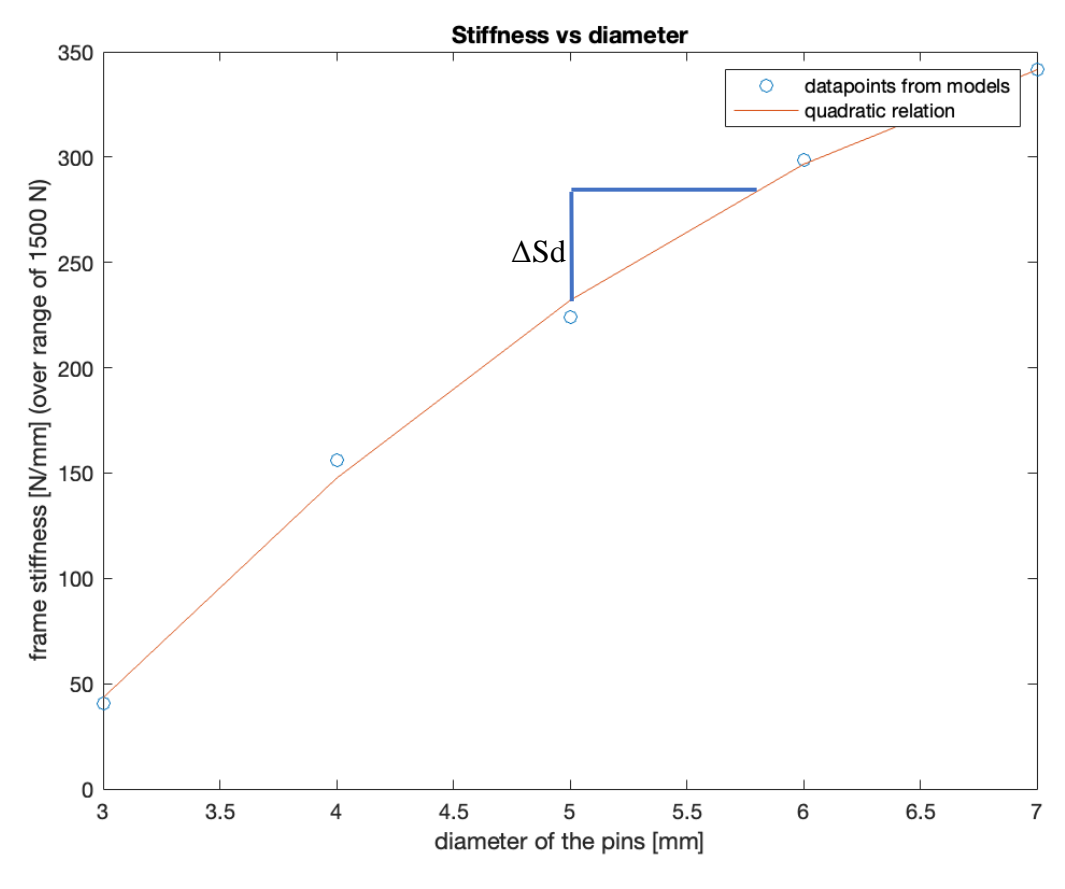








Appendix Figure 6 Determination of the ΔSl in the quadratic relation of average pin length vs the stiffness of the construct.



Appendix Figure 7 Determination of the ΔSd in the quadratic relation of average pin length vs the stiffness of the construct.





